AD-A268 350

Atlas of Formability

Inconel 718

DTIC
SELECTE
AUG 18 1993
S B D
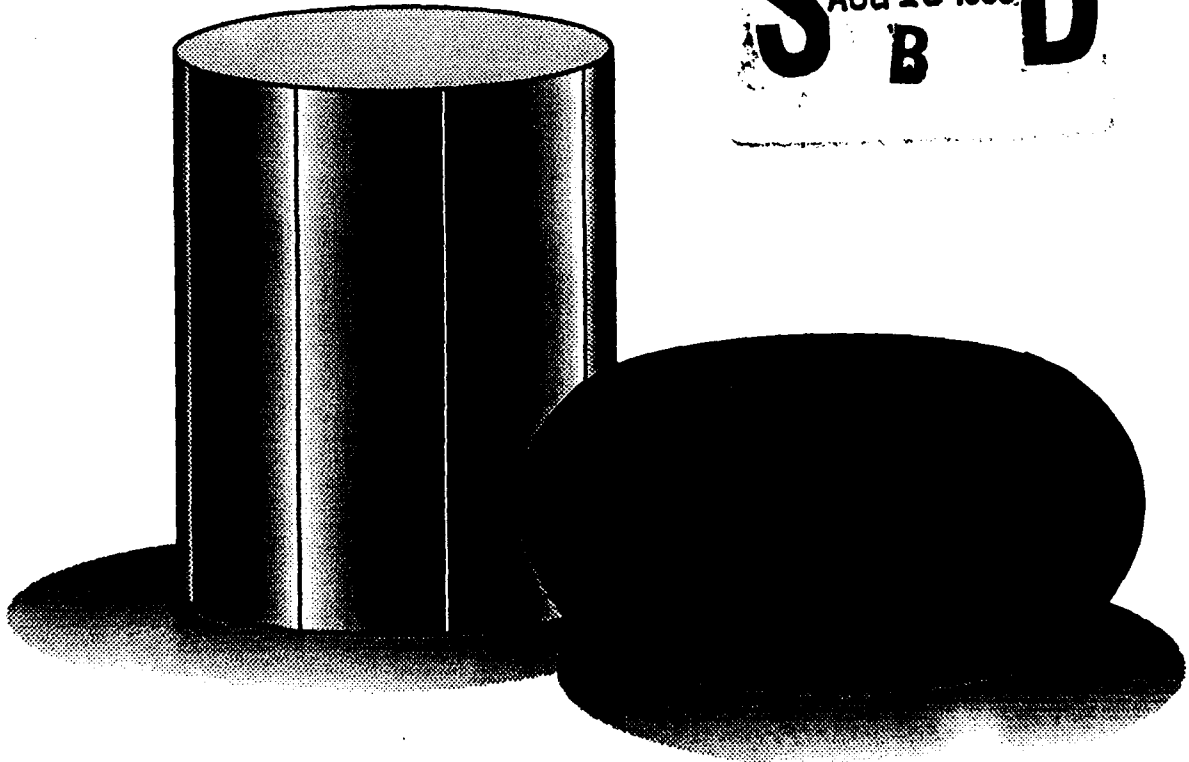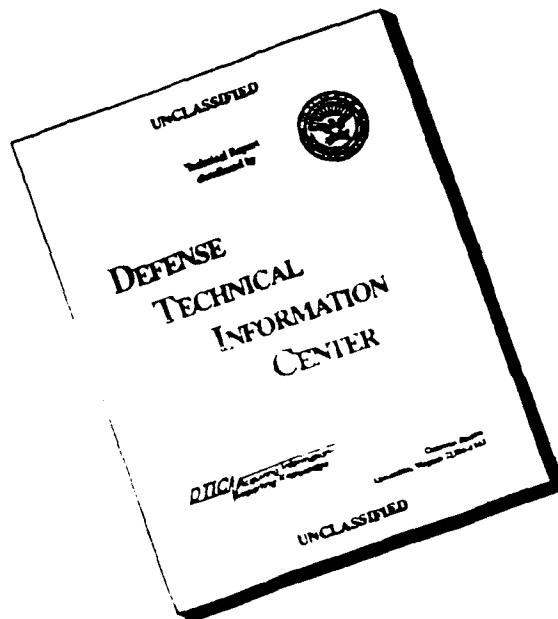
93-18968

NCEMT

DISCLAIMER NOTICE

THIS DOCUMENT IS BEST QUALITY AVAILABLE. THE COPY FURNISHED TO DTIC CONTAINED A SIGNIFICANT NUMBER OF PAGES WHICH DO NOT REPRODUCE LEGIBLY.

REPORT DOCUMENTATION PAGE

Public reporting burden for this collection of information is estimated to average 1 hour per response, including the time for reviewing instructions, searching existing data sources, gathering and maintaining the data needed, and completing and reviewing the collection of information. Send comments regarding this burden estimate or any other aspect of this collection of information, including suggestions for reducing this burden, to Washington Headquarters Services, Directorate for Information Operations and Reports, 1215 Jefferson Davis Highway, Suite 1204, Arlington, VA 22202-4302, and to the Office of Management and Budget, Paperwork Reduction Project (0704-0188), Washington, DC 20503.

1. AGENCY USE ONLY (Leave blank)	2. REPORT DATE	3. REPORT TYPE AND DATES COVERED
	July 31, 1992	Final, April 30, 1992-July 31, 1992

4. TITLE AND SUBTITLE

Atlas of Formability
Inconel 718

5. FUNDING NUMBERS

C-N00140-88-C-RC21

6. AUTHOR(S)

Prabir K. Chaudhury
Dan Zhao

7. PERFORMING ORGANIZATION NAME(S) AND ADDRESS(ES)

National Center for Excellence in Metalworking
Technology (NCEMT)
1450 Scalp Avenue
Johnstown, PA 15904

8. PERFORMING ORGANIZATION REPORT NUMBER

9. SPONSORING/MONITORING AGENCY NAME(S) AND ADDRESS(ES)

Naval Industrial Resources Support Activity
Building 75-2, Naval Base
Philadelphia, PA 19112-5078

10. SPONSORING/MONITORING AGENCY REPORT NUMBER

11. SUPPLEMENTARY NOTES

12a. DISTRIBUTION/AVAILABILITY STATEMENT

12b. DISTRIBUTION CODE

13. ABSTRACT (Maximum 200 words)

In this investigation, flow behavior of Inconel 718 alloy was studied by conducting compression tests over a wide range of temperatures and strain rates. Constitutive relations were determined from the flow behavior, and a dynamic material modeling was conducted on this alloy. Thus, the optimum processing condition in terms of temperature and strain rate was identified. Microstructural changes during high temperature deformation were also characterized.

14. SUBJECT TERMS

15. NUMBER OF PAGES

16. PRICE CODE

17. SECURITY CLASSIFICATION OF REPORT	18. SECURITY CLASSIFICATION OF THIS PAGE	19. SECURITY CLASSIFICATION OF ABSTRACT	20. LIMITATION OF ABSTRACT
Unclassified	Unclassified	Unclassified	

GENERAL INSTRUCTIONS FOR COMPLETING SF 298

The Report Documentation Page (RDP) is used in announcing and cataloging reports. It is important that this information be consistent with the rest of the report, particularly the cover and title page. Instructions for filling in each block of the form follow. It is important to *stay within the lines* to meet *optical scanning requirements*.

Block 1. Agency Use Only (Leave blank).

Block 2. Report Date. Full publication date including day, month, and year, if available (e.g. 1 Jan 88). Must cite at least the year.

Block 3. Type of Report and Dates Covered. State whether report is interim, final, etc. If applicable, enter inclusive report dates (e.g. 10 Jun 87 - 30 Jun 88).

Block 4. Title and Subtitle. A title is taken from the part of the report that provides the most meaningful and complete information. When a report is prepared in more than one volume, repeat the primary title, add volume number, and include subtitle for the specific volume. On classified documents enter the title classification in parentheses.

Block 5. Funding Numbers. To include contract and grant numbers; may include program element number(s), project number(s), task number(s), and work unit number(s). Use the following labels:

C	-	Contract	PR	-	Project
G	-	Grant	TA	-	Task
PE	-	Program Element	WU	-	Work Unit Accession No.

Block 6. Author(s). Name(s) of person(s) responsible for writing the report, performing the research, or credited with the content of the report. If editor or compiler, this should follow the name(s).

Block 7. Performing Organization Name(s) and Address(es). Self-explanatory.

Block 8. Performing Organization Report Number. Enter the unique alphanumeric report number(s) assigned by the organization performing the report.

Block 9. Sponsoring/Monitoring Agency Name(s) and Address(es). Self-explanatory.

Block 10. Sponsoring/Monitoring Agency Report Number. *(If known)*

Block 11. Supplementary Notes. Enter information not included elsewhere such as: Prepared in cooperation with...; Trans. of...; To be published in.... When a report is revised, include a statement whether the new report supersedes or supplements the older report.

Block 12a. Distribution/Availability Statement. Denotes public availability or limitations. Cite any availability to the public. Enter additional limitations or special markings in all capitals (e.g. NOFORN, REL, ITAR).

DOD	-	See DoDD 5230.24, "Distribution Statements on Technical Documents."
DOE	-	See authorities.
NASA	-	See Handbook NHB 2200.2.
NTIS	-	Leave blank.

Block 12b. Distribution Code.

DOD	-	Leave blank.
DOE	-	Enter DOE distribution categories from the Standard Distribution for Unclassified Scientific and Technical Reports.
NASA	-	Leave blank.
NTIS	-	Leave blank.

Block 13. Abstract. Include a brief *(Maximum 200 words)* factual summary of the most significant information contained in the report.

Block 14. Subject Terms. Keywords or phrases identifying major subjects in the report.

Block 15. Number of Pages. Enter the total number of pages.

Block 16. Price Code. Enter appropriate price code *(NTIS only)*.

Blocks 17. - 19. Security Classifications. Self-explanatory. Enter U.S. Security Classification in accordance with U.S. Security Regulations (i.e., UNCLASSIFIED). If form contains classified information, stamp classification on the top and bottom of the page.

Block 20. Limitation of Abstract. This block must be completed to assign a limitation to the abstract. Enter either UL (unlimited) or SAR (same as report). An entry in this block is necessary if the abstract is to be limited. If blank, the abstract is assumed to be unlimited.

ATLAS OF FORMABILITY

INCONEL 718

by

Prabir K. Chaudhury and Dan Zhao

National Center for Excellence in Metalworking Technology
1450 Scalp Avenue
Johnstown, PA 15904

for

July 31, 1992

The views, opinions, and/or findings contained in this report are those of the authors and should not be construed as an official Department of the Navy position, policy, or decision, unless so designated by other documentation

TABLE OF CONTENTS

DTIC QUALITY INSPECTED 3

LIST OF TABLE

Inconel 718

Introduction

Among the commercially available superalloys, Inconel 718 stands out as the most dominant alloy in production. High performance requirements in the application of superalloys, such as aircraft gas turbines, has increased the need to understand the behavior of superalloys. At the same time modern metalworking processes require a better knowledge of mechanical and microstructural behavior during high temperature deformation. Flow behavior of Inconel 718 was studied by conducting compression tests at various temperatures and strain rates to determine the constitutive relation. From the constitutive relation a dynamic material modeling on Inconel 718 was carried out to optimize processing conditions in terms of temperature and strain rate. In addition, microstructural changes were characterized to show the effect of the deformation on the resulting microstructure.

Experimental Procedure

The material used in this investigation was commercially available Inconel 718 wrought bars in heat treated and aged condition. The typical microstructure of the as-received materials is shown in Figure 1 showing equiaxed grains. The initial grain size is 23 μm (7.5ASTM). Cylindrical compression test specimens with a diameter of 12.7 mm and a height of 15.9 mm were machined, and compression tests were conducted isothermally on an MTS testing machine. The temperatures selected include those which are both above and under δ (1038 C) solvus. The test matrix was as follows:

Temperature, C (F): 982 (1800), 1010 (1850), 1038 (1900), 1079 (1975) and 1149 (2100);
Strain rate, s^{-1}: 0.01, 0.14, 1.84, 5 and 25.

The tests were conducted in air except the ones at strain rate of 5 s^{-1}, which were conducted in inert gas atmosphere. Load and stroke data from the tests were acquired by a computer and later converted to true stress-true strain curves. Immediately after the compression test, the specimens were quenched in order to retain the deformed microstructure. Longitudinal and transverse sections of the quenched specimens were examined using optical microscope. The photomicrographs presented were taken from the center of the longitudinal section of the specimens.

Results

Table 1 is a list of the figures, test conditions and the observed microstructures. All the true stress-true strain flow curves with the corresponding deformed microstructure are shown in Figure 2 to Figure 26. True stress versus strain rate was plotted in log-log scale in Figure 27 at a true strain of 0.3. The slope of the plot gives the strain rate sensitivity m, which is not a constant over the range of strain rate tested. Log stress vs. 1/T at the same true strain is shown in Figure 28. Processing map at this strain was developed for Inconel 718, Figure 29. The optimum processing conditions from the map can be obtained by selecting the temperature and strain rate combination which provides the maximum efficiency in the stable region. This condition is approximately 1070 C and 0.01 s^{-1} for Inconel 718.

Table 1. List of figures, testing conditions and microstructural observations for Inconel 718.

| Figure No	Temperature C(F)	Strain Rate S-1	Microstructure Optical Microscopy	Page No
1			Heat treated and aged wrought bars. Equiaxed grains of ~23μm (7.5ASTM).	3
2	982(1800)	0.01	Deformed grains showing serrated grain boundaries (initiation of dynamic recrystallization), incipient necklacing.	4
3	982(1800)	0.14	Same as above, but the grains appeared to be more severely deformed.	5
4	982(1800)	1.84	Small and equiaxed dynamically recrystallized grains (~7μm).	6
5	982(1800)	5	Same as above, but the grains are smaller (~5.6μm), a very small proportion of deformed grains still present, tested in an inert atmosphere.	7
6	982(1800)	25	n/a	8
7	1010(1850)	0.01	Deformed grains showing serrated grain boundaries , necklacing present.	9
8	1010(1850)	0.14	Equiaxed dynamically recrystallized grains with an average size of 6.5μm.	10
9	1010(1850)	1.84	Equiaxed grains with an average size of 10.6μm, twinning present.	11
10	1010(1850)	5	Equiaxed grains with a duplex structure; small grains 4-8μm and large grains 20-30μm. Small fraction of large deformed grains is also present, tested in an inert atmosphere.	12
11	1010(1850)	25	Equiaxed grains with an average size of 7.6μm.	13
12	1038(1900)	0.01	Equiaxed grains (~17μm) developing twins. Note that 1038 C is just bellow the δ solvus.	14
13	1038(1900)	0.14	Equiaxed grains with an average size of 10μm.	15
14	1038(1900)	1.84	Equiaxed grains (~12μm) developing twins.	16
15	1038(1900)	5	Equiaxed grains with a duplex structure; small grains ~12μm and large grains 25-30μm. Small fraction of large deformed grains is also present, tested in an inert atmosphere.	17
16	1038(1900)	25	Same as above, but the grains are slightly smaller, tested in an inert atmosphere.	18
17	1079(1975)	0.01	Large duplex equiaxed grains with a grain size in the range of 40-60 μm. Tested in an inert atmosphere.	19
18	1079(1975)	0.14	Equiaxed large grains with a duplex size	20
19	1079(1975)	1.84	Equiaxed grains (22-30μm) developing twins.	21
20	1079(1975)	5	Equiaxed grains (~29μm), tested in an inert atmosphere.	22
21	1079(1975)	25	Equiaxed grains (22-25μm).	23
22	1149(2100)	0.01	Large equiaxed grains (~61μm).	24
23	1149(2100)	0.14	Same as above, but smaller grains	25
24	1149(2100)	1.84	Large equiaxed grains.	26
25	1149(2100)	5	Equiaxed grains (~56μm), tested in an inert atmosphere.	27
26	1149(2100)	25	Equiaxed grains (~41μm)	28
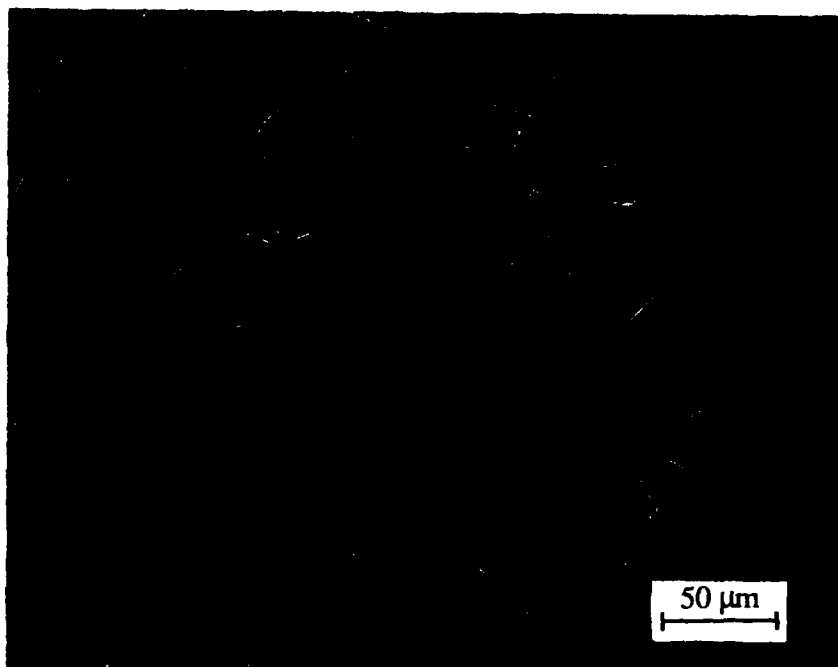
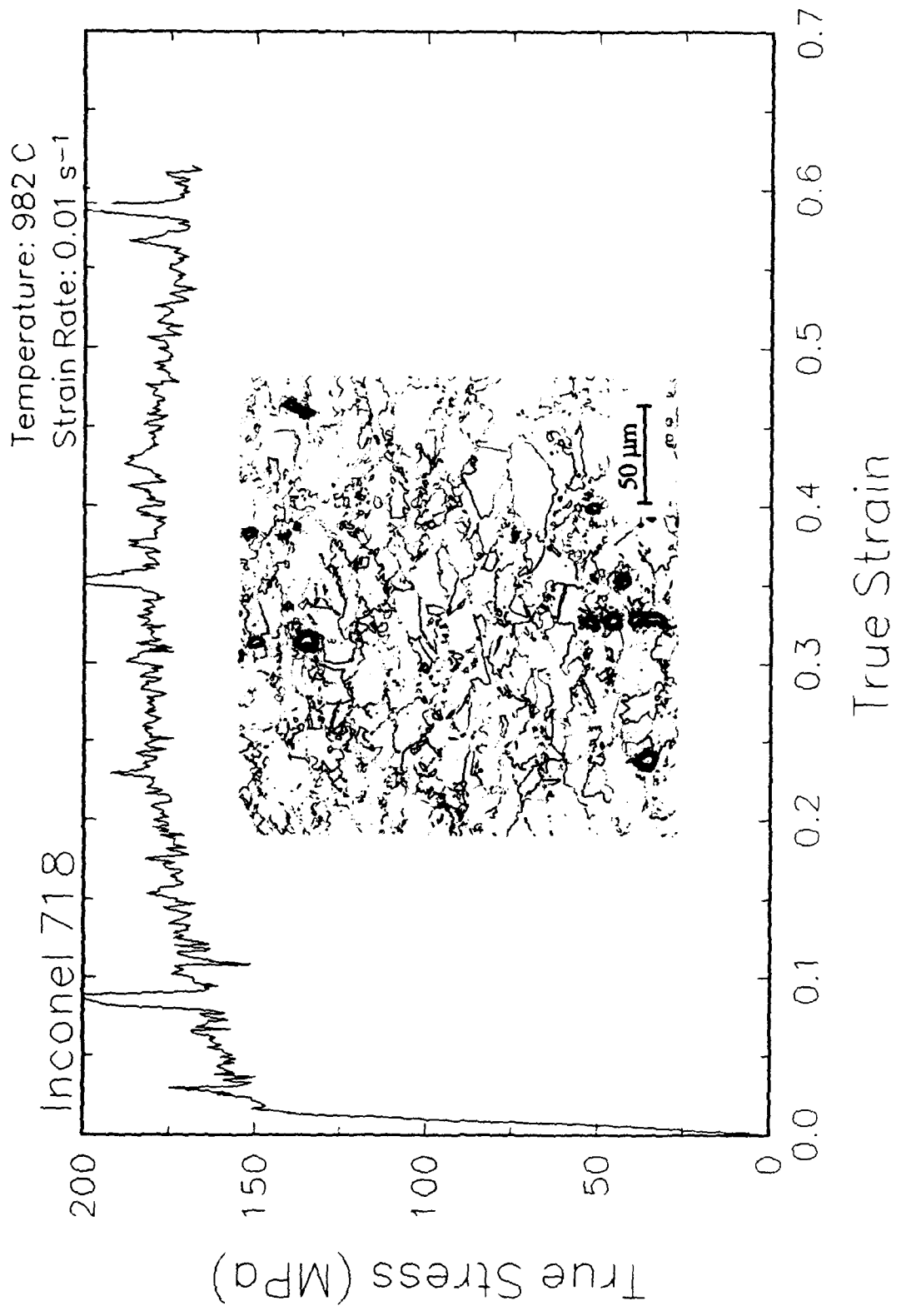Figure 1. As-received microstructure of Inconel 718.

Figure 2. True stress-true strain curve and microstructure at 982 C and 0.01 s⁻¹.
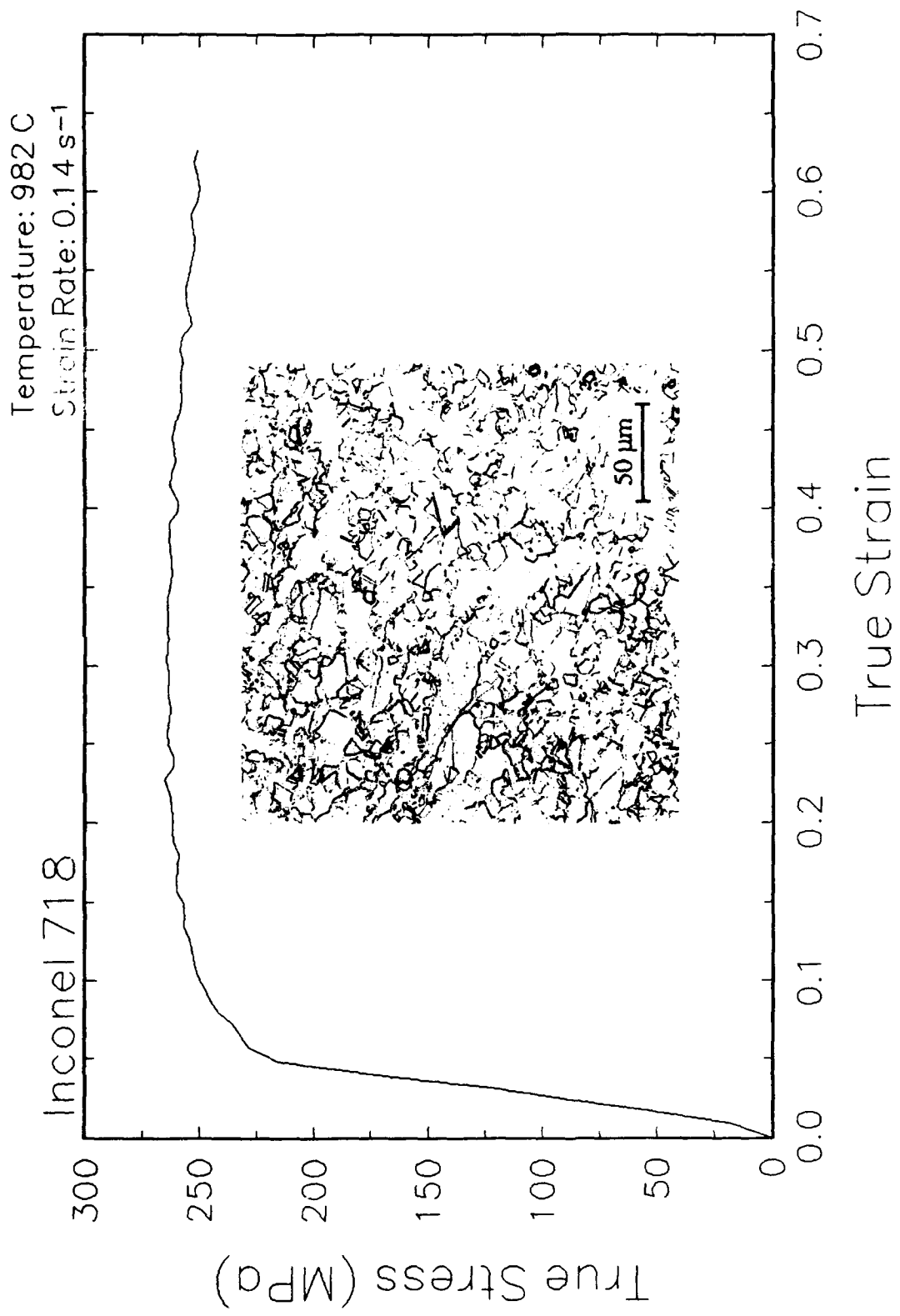
Figure 3. True stress-true strain curve and microstructure at 982 C and 0.14 s⁻¹.
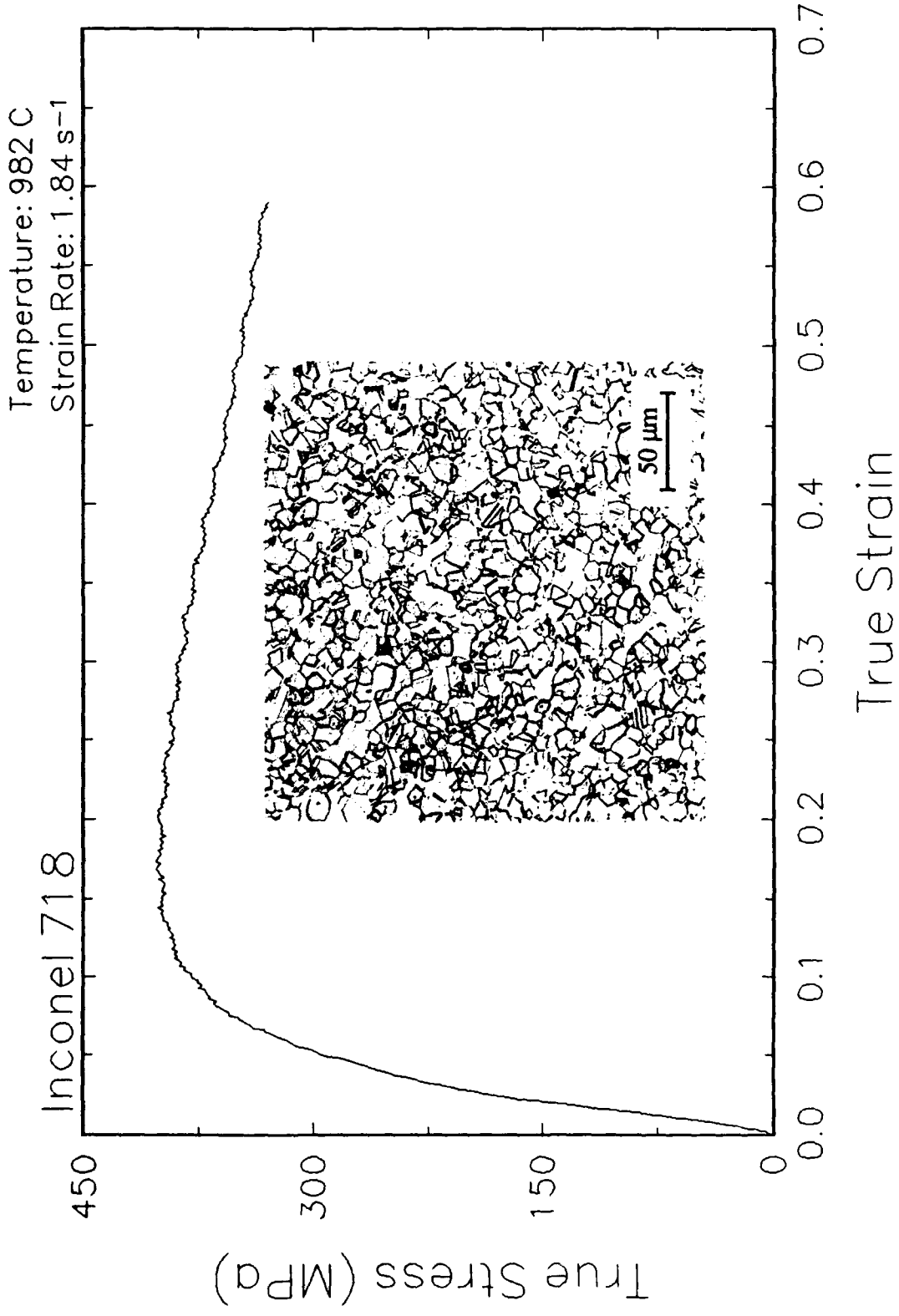
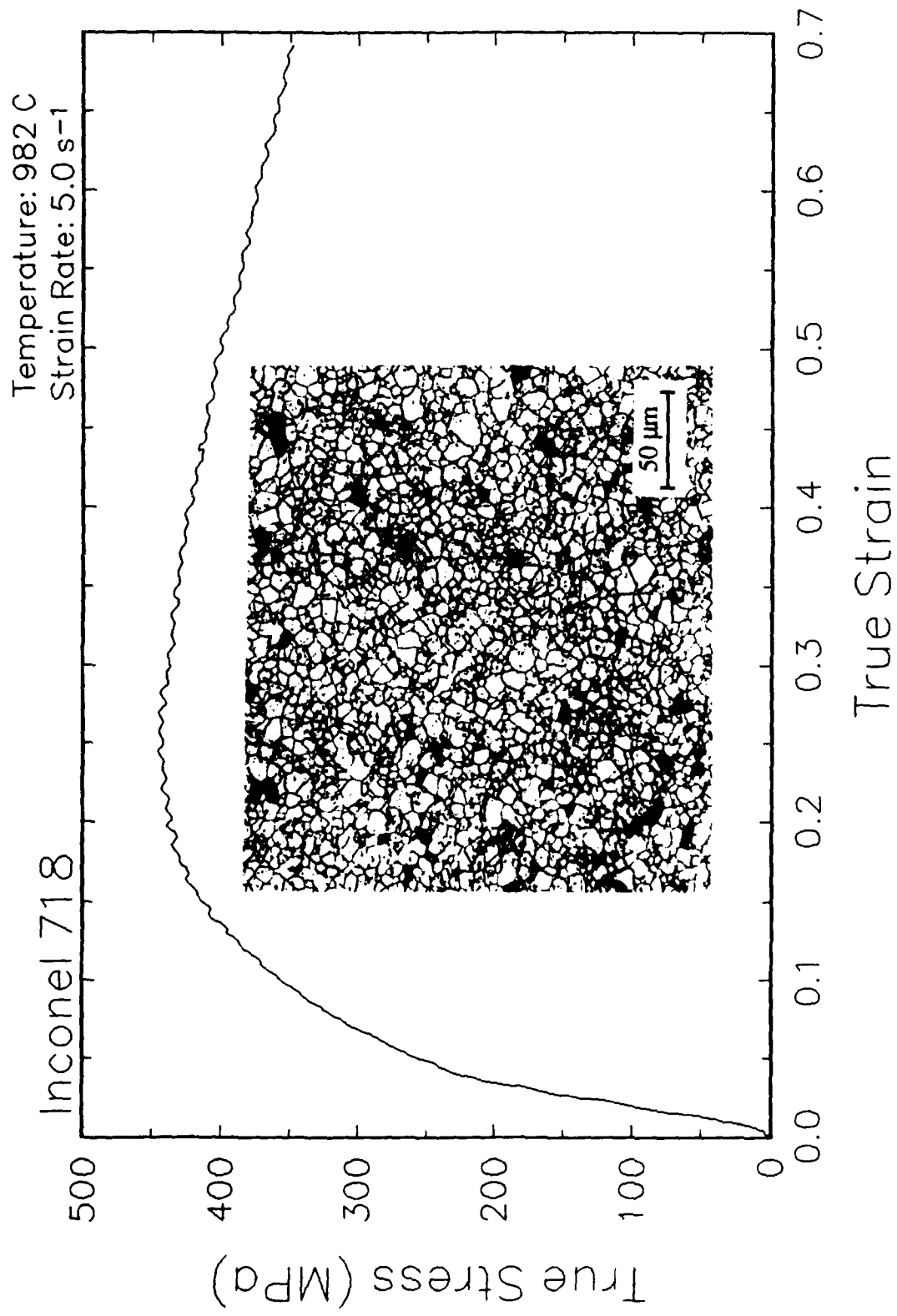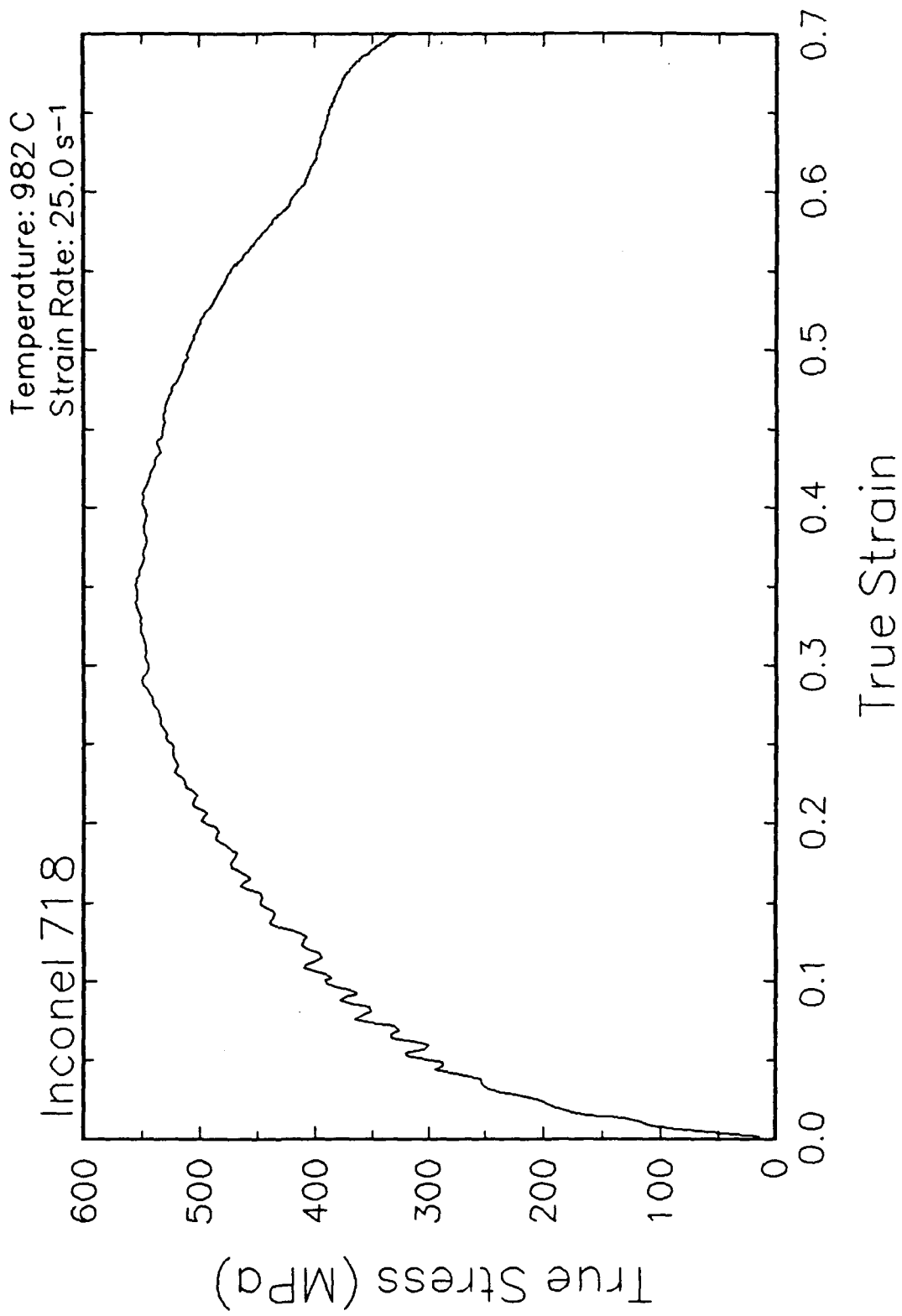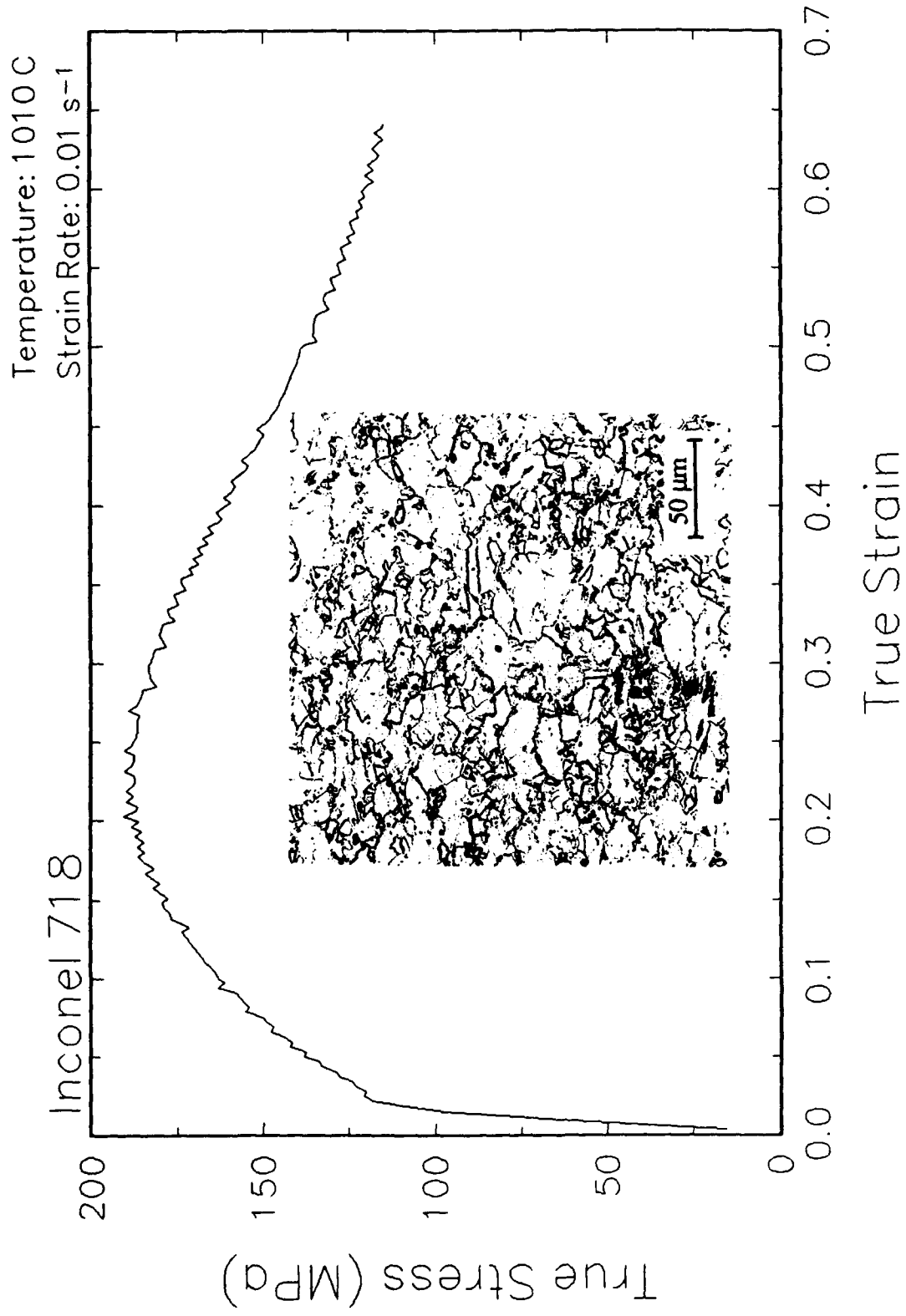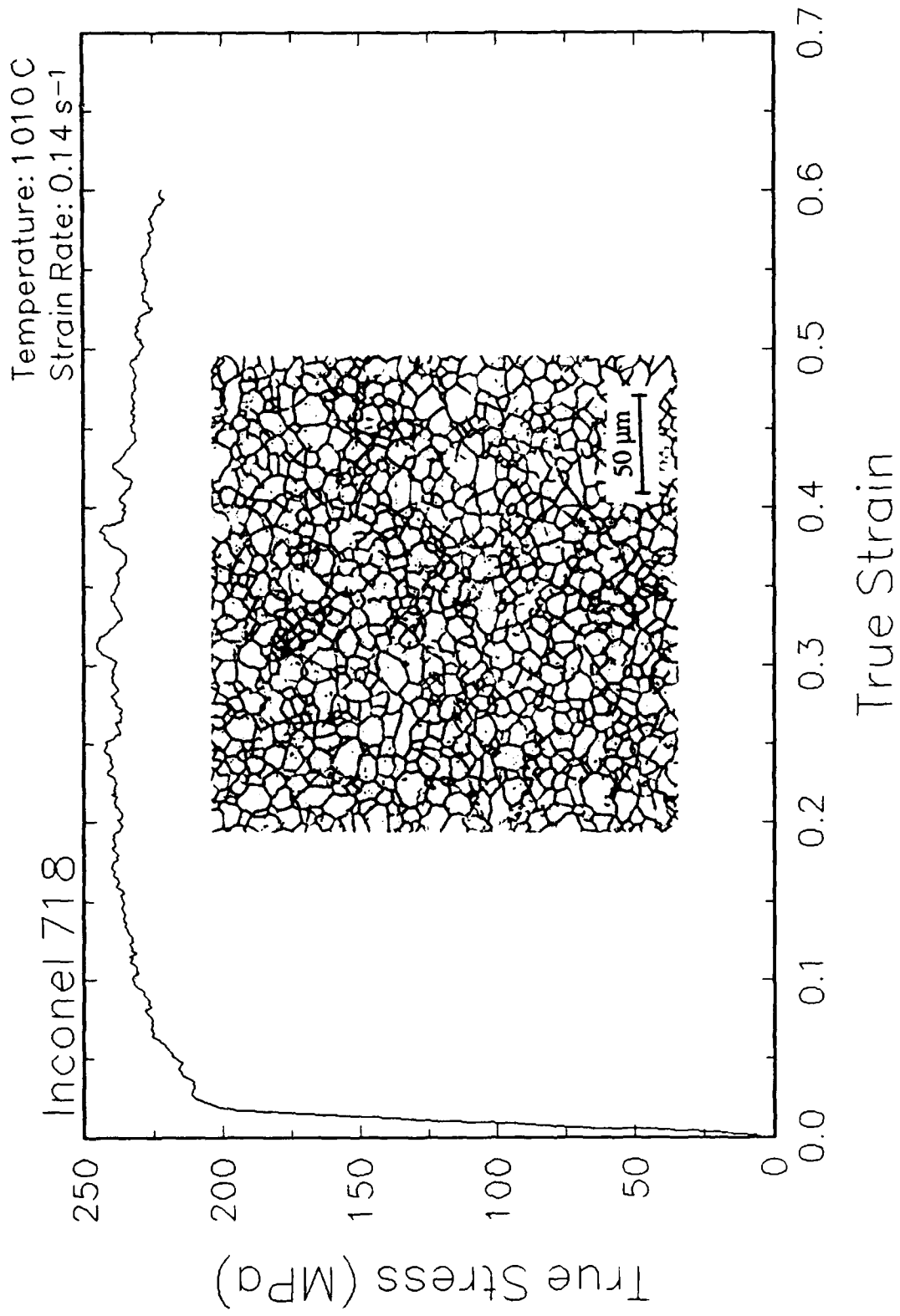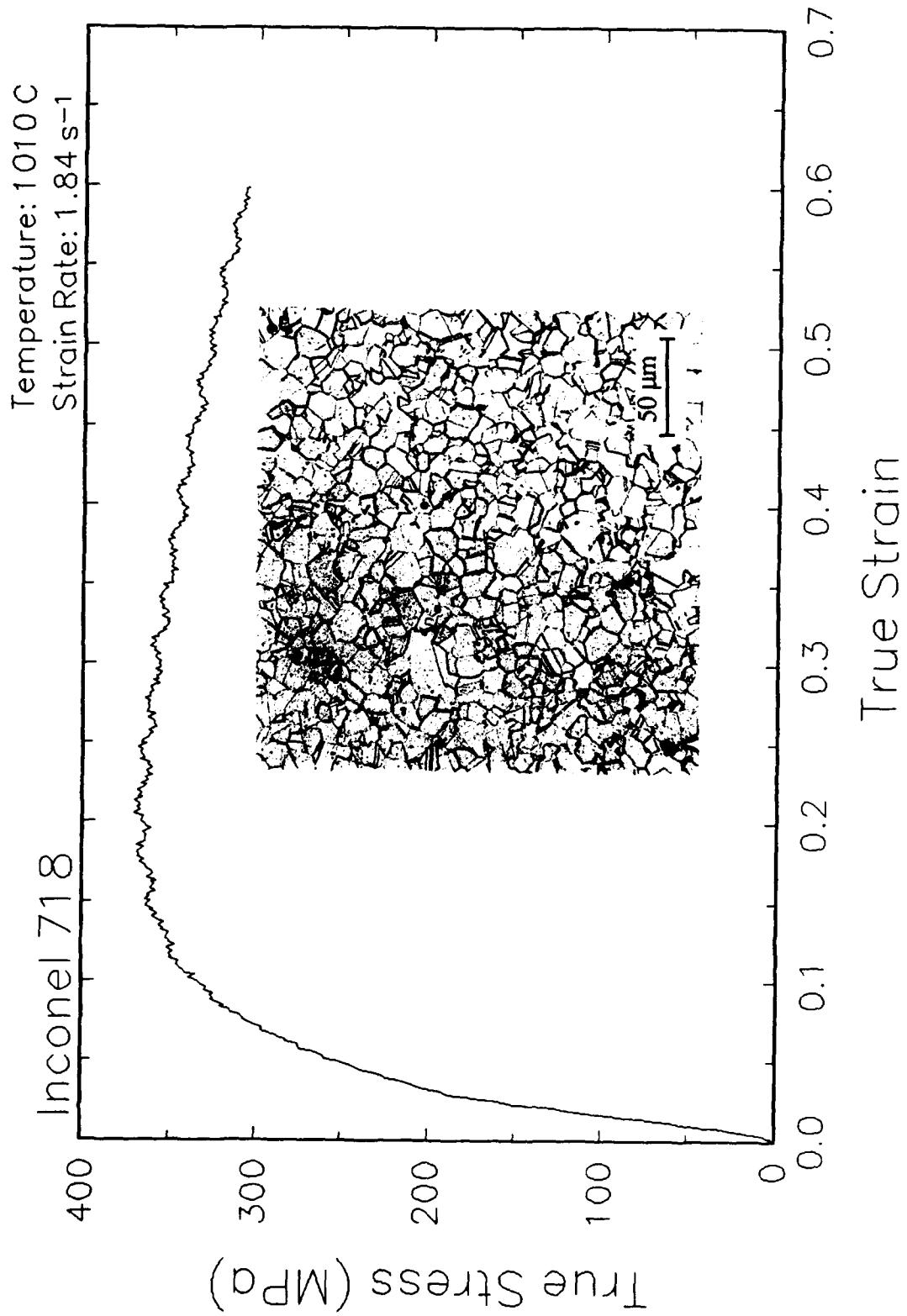**Figure 4. True stress-true strain curve and microstructure at 982 C and 1.84 s^{-1}.**
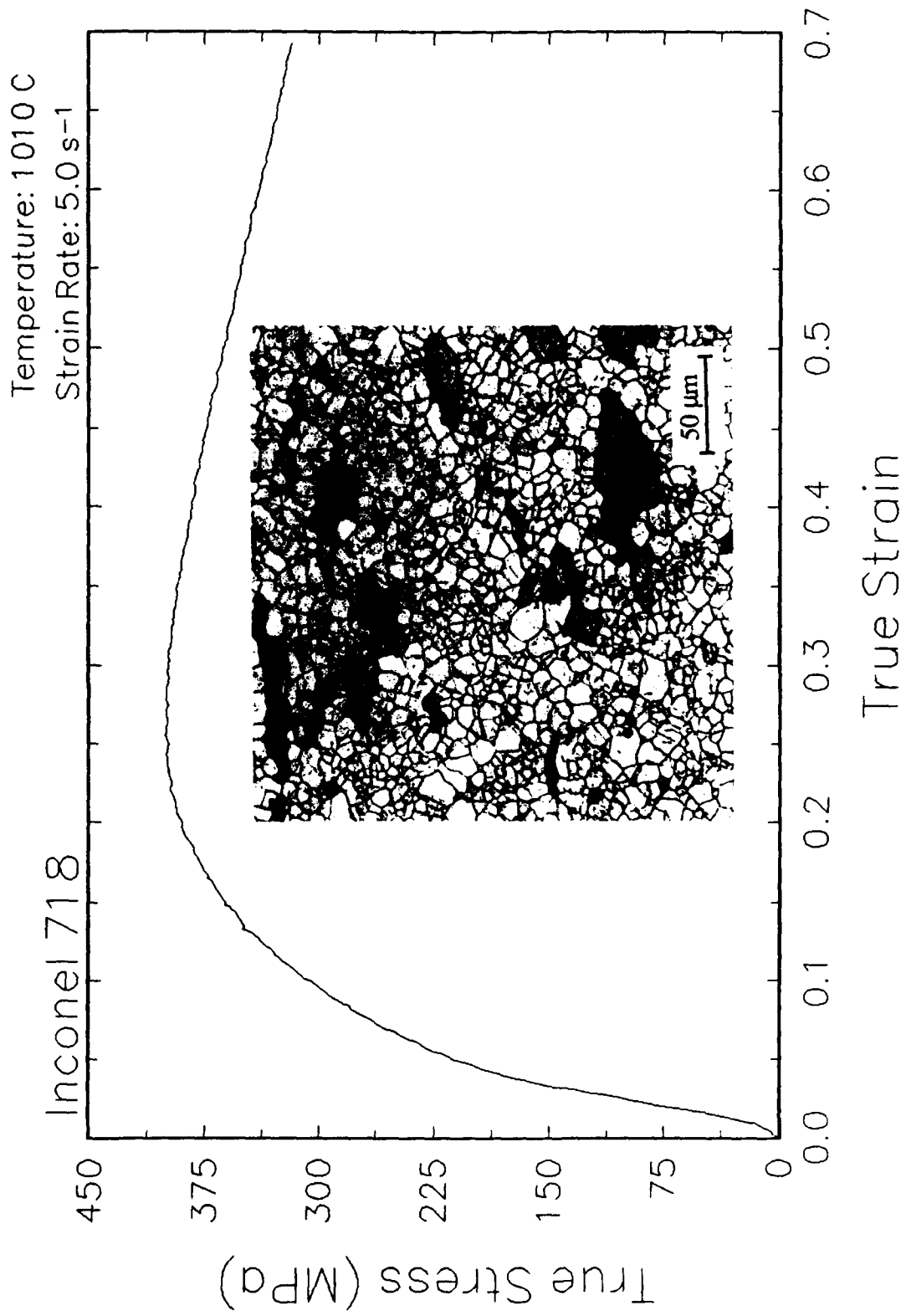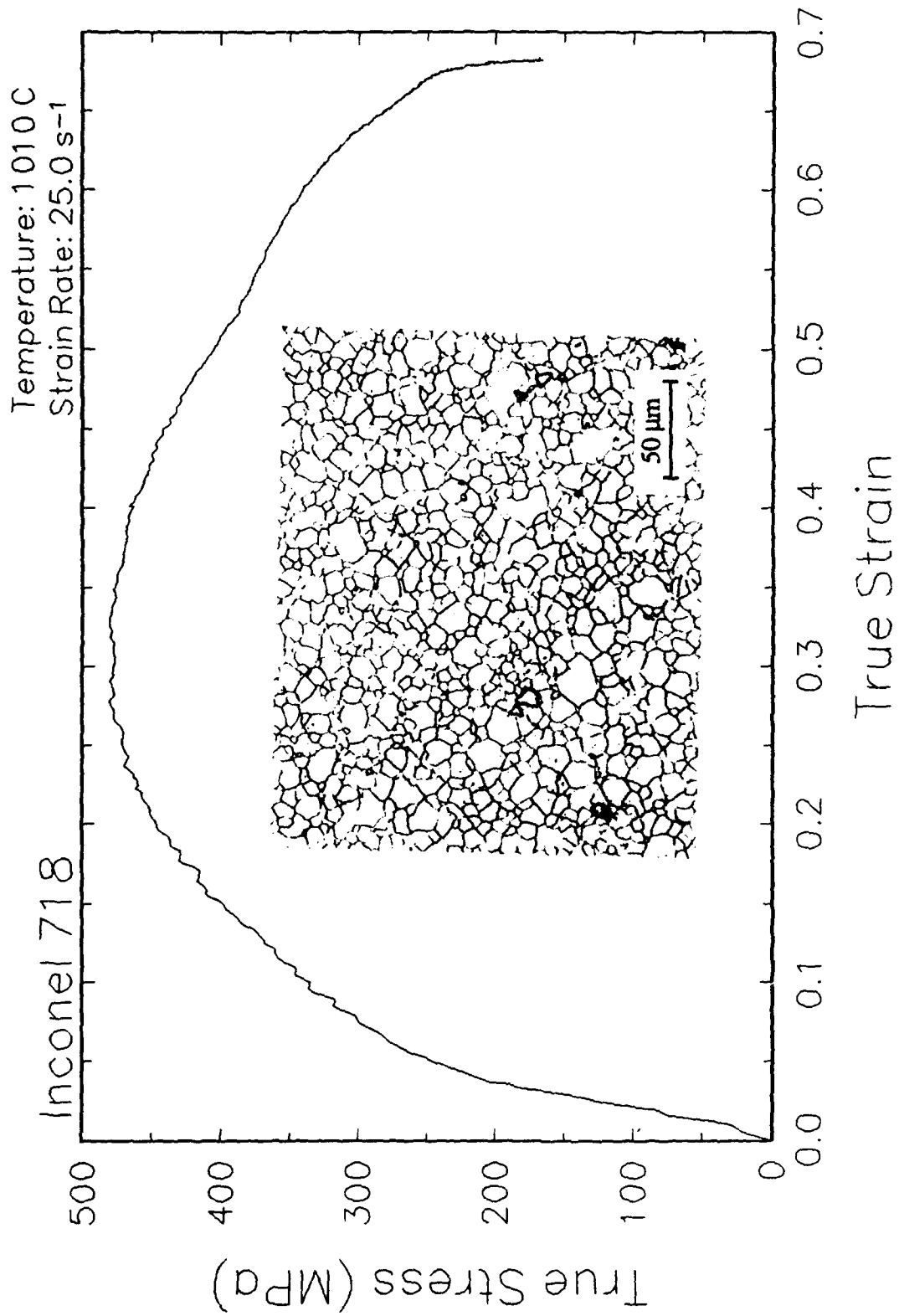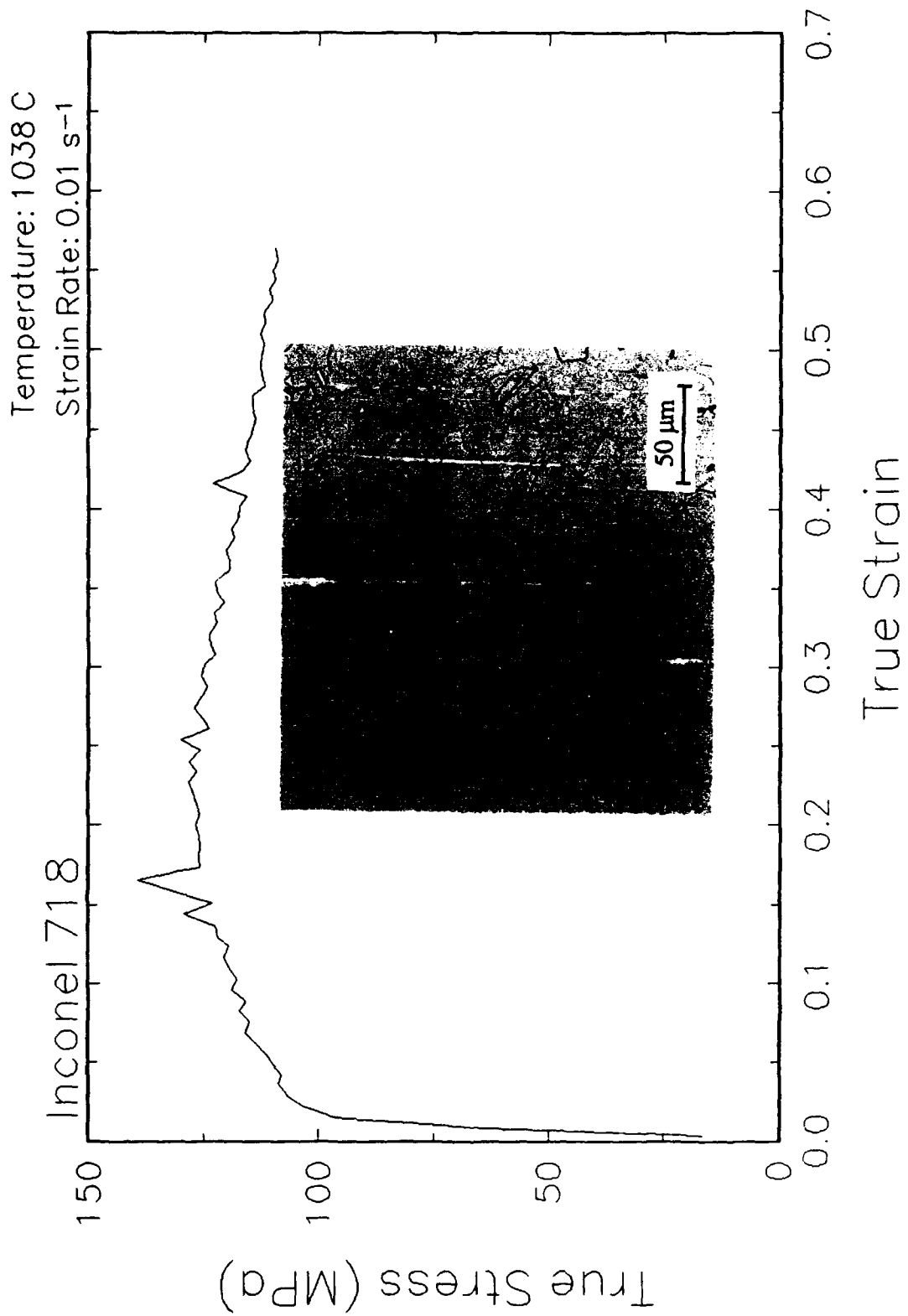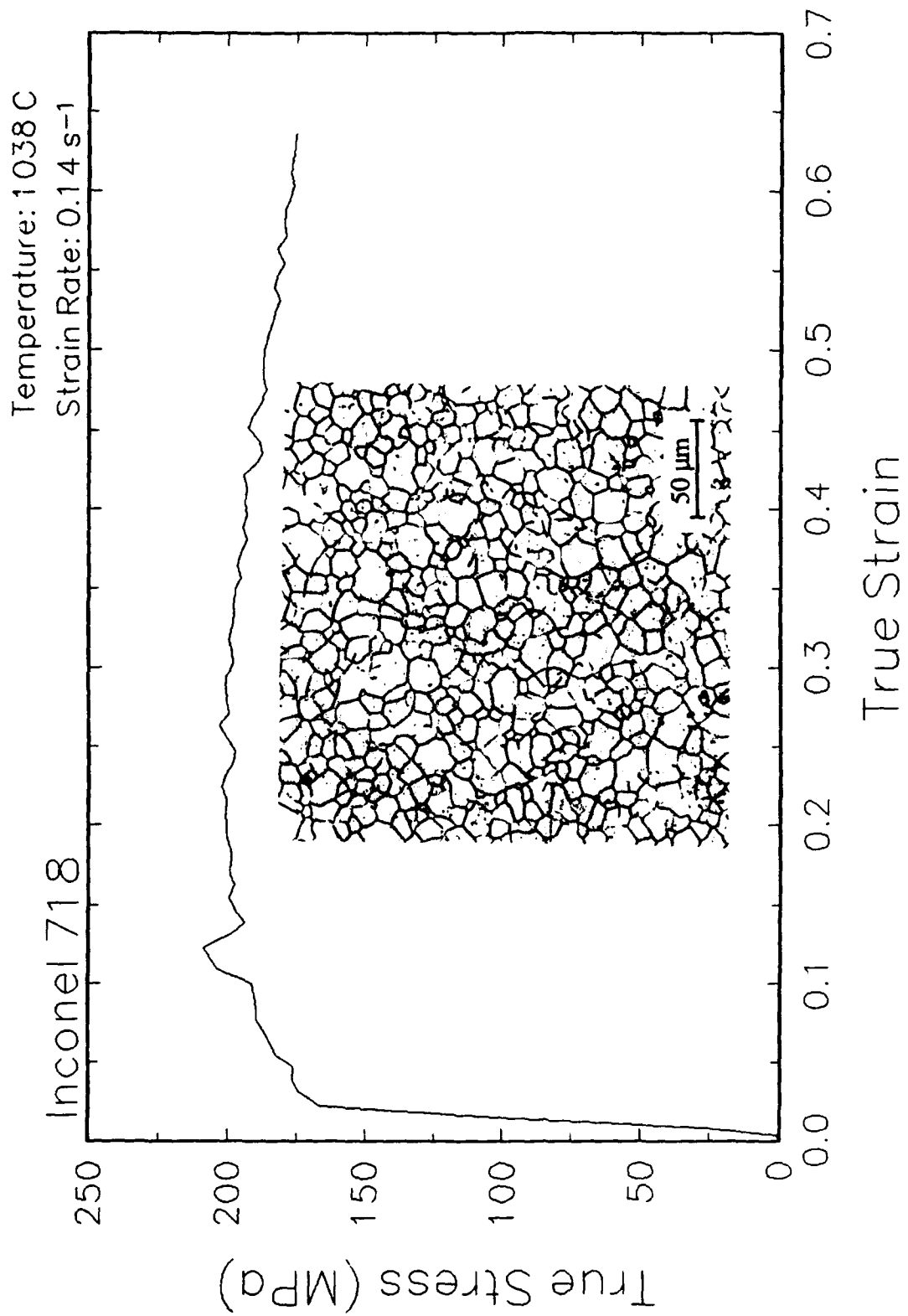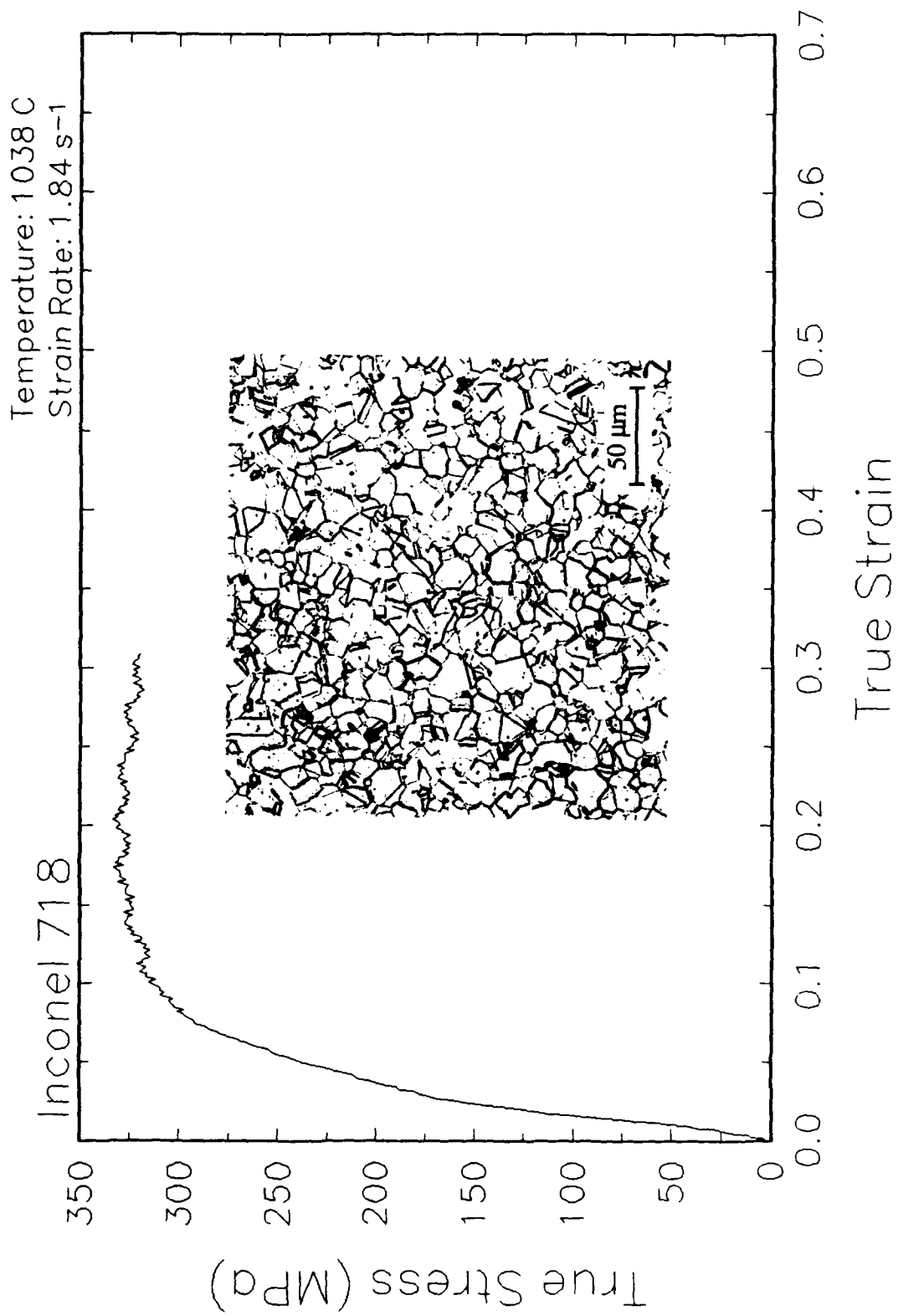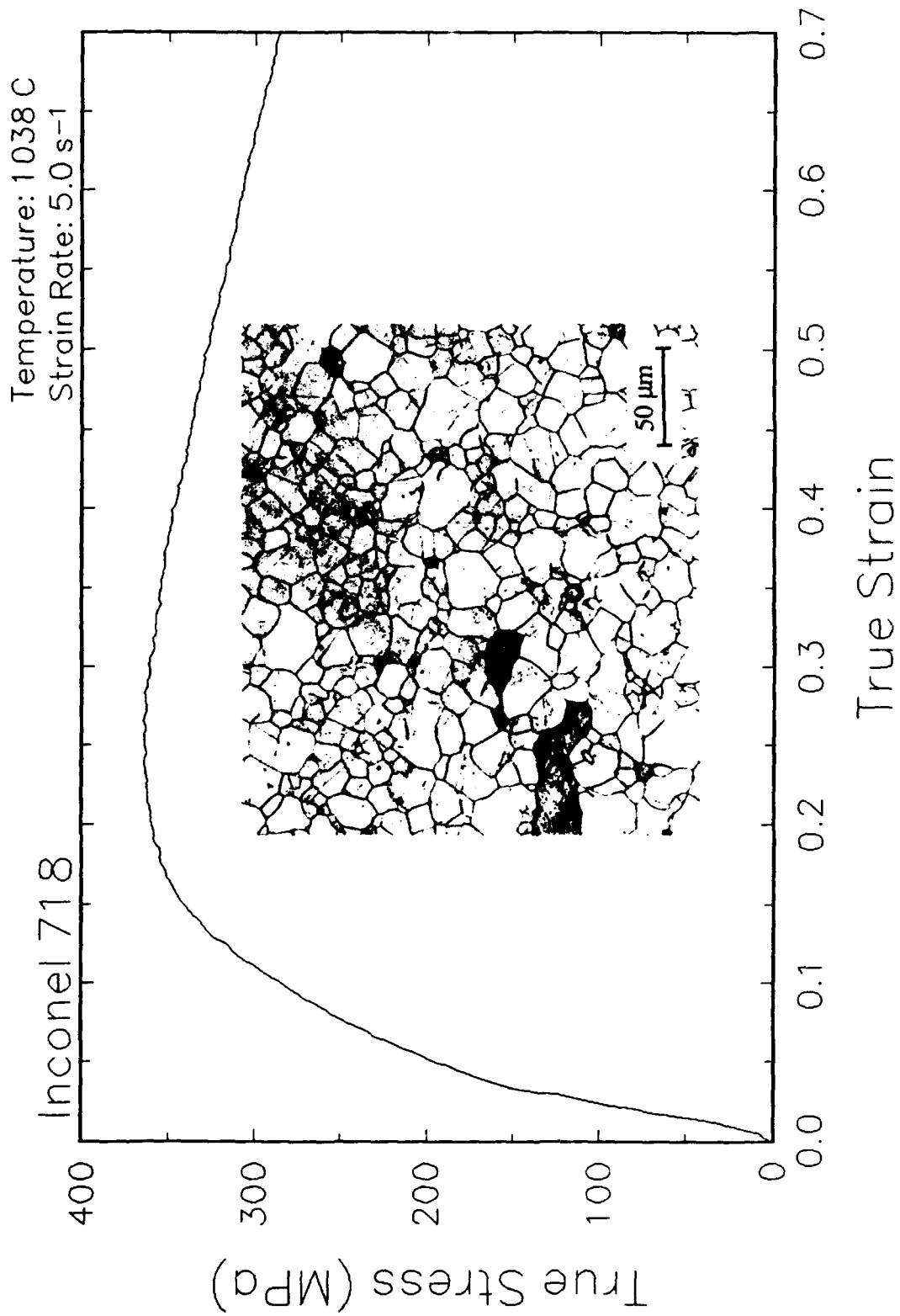
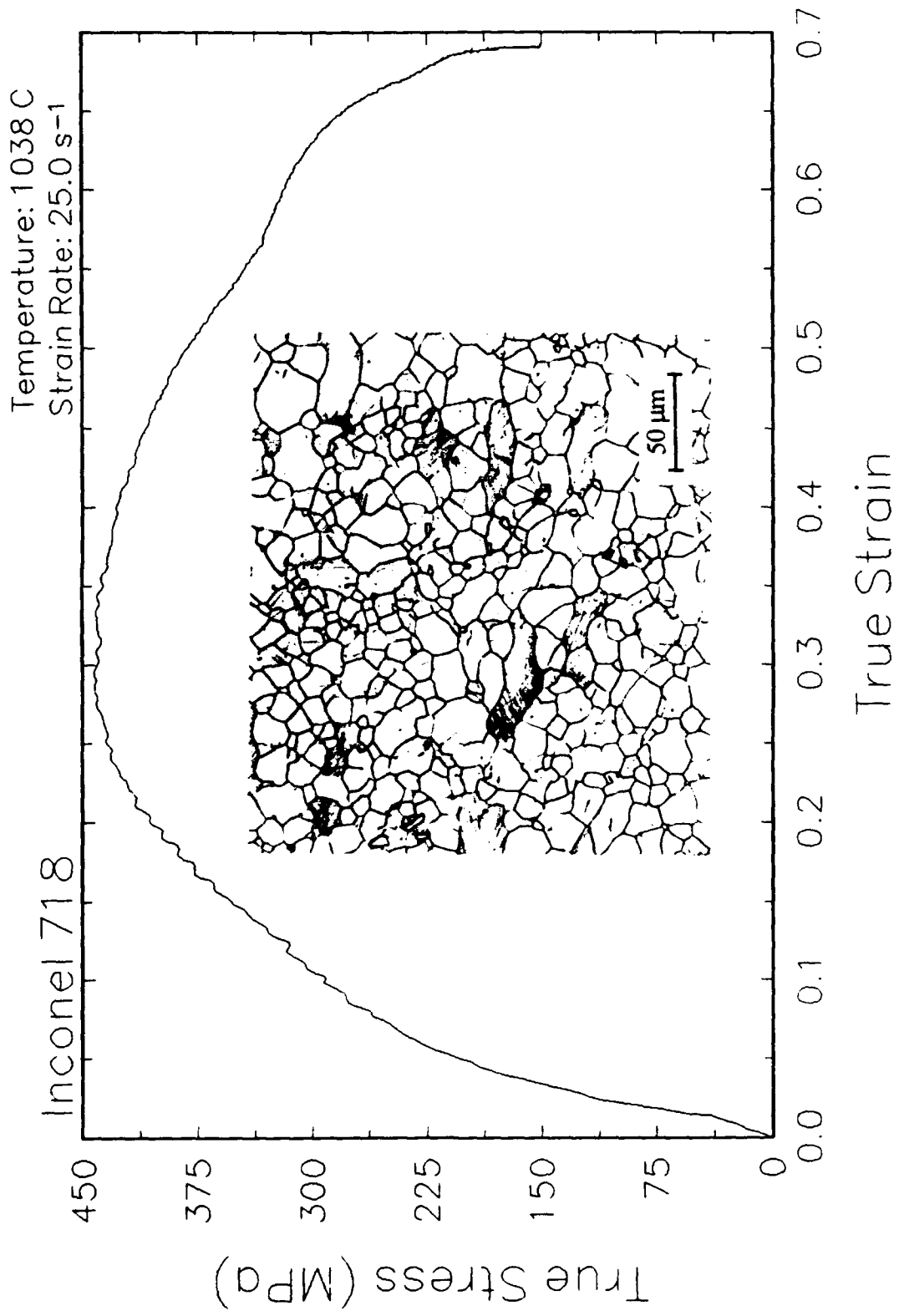**Figure 5.** True stress-true strain curve and microstructure at 982 C and 5 s⁻¹.

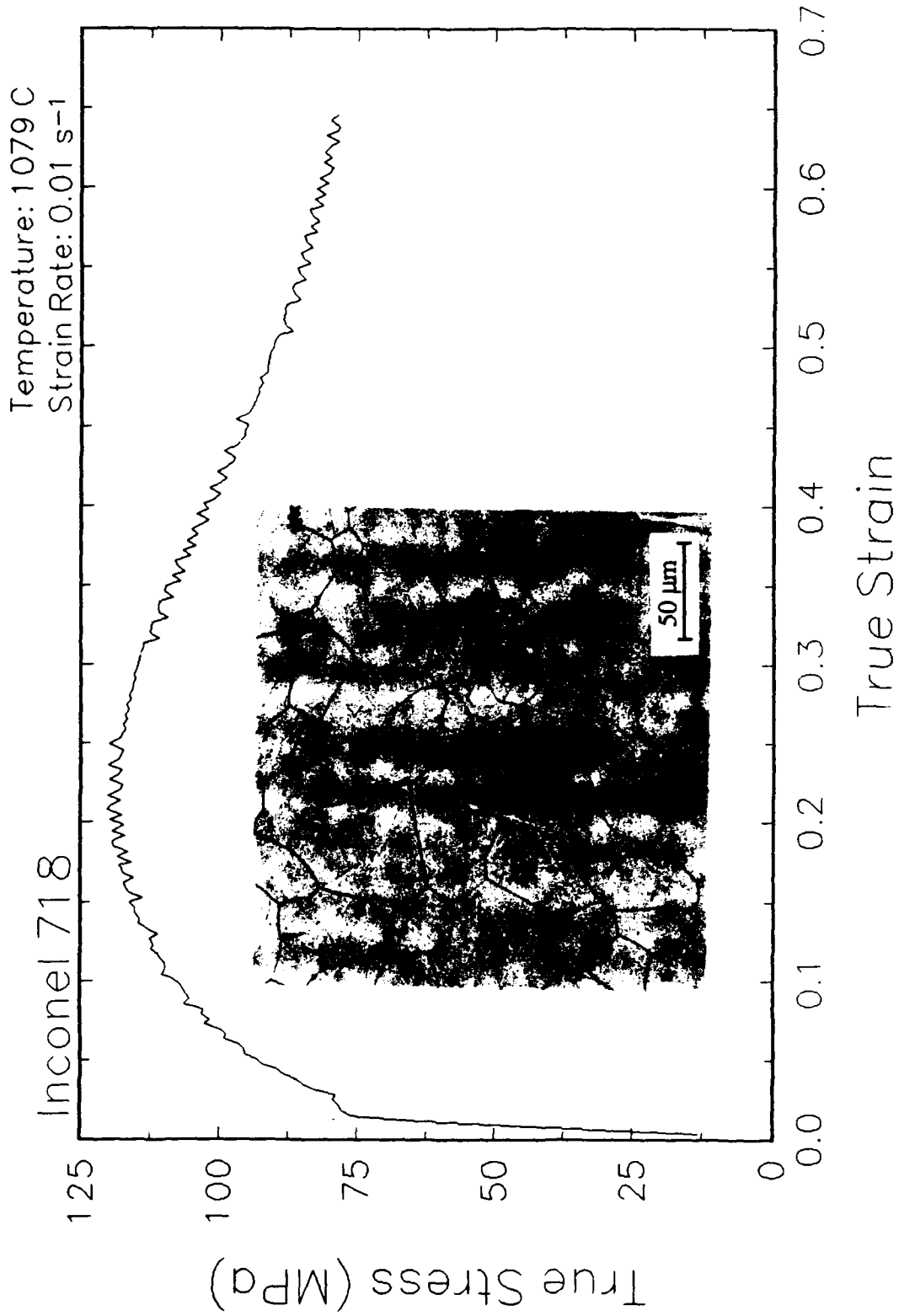**Figure 6.** True stress-true strain curve and microstructure at 982 C and 25 s⁻¹.

Figure 7. True stress-true strain curve and microstructure at 1010 C and 0.01 s⁻¹.

Figure 8. True stress-true strain curve and microstructure at 1010 C and 0.14 s^{-1}.

Figure 9. True stress-true strain curve and microstructure at 1010 C and 1.84 s⁻¹.

Figure 10. True stress-true strain curve and microstructure at 1010 C and 5 s⁻¹.

Figure 11. True stress-true strain curve and microstructure at 1010 C and 25 s⁻¹.

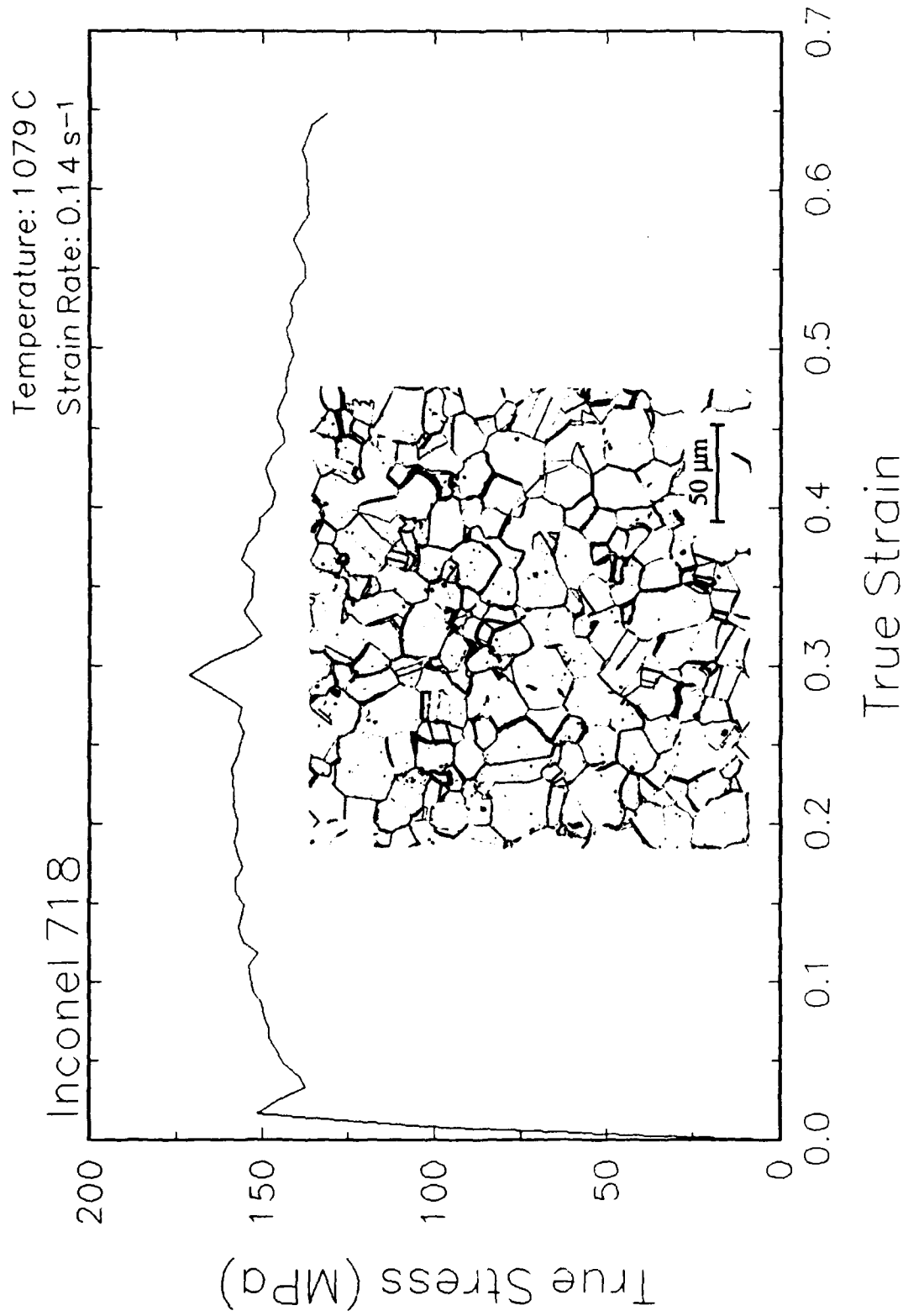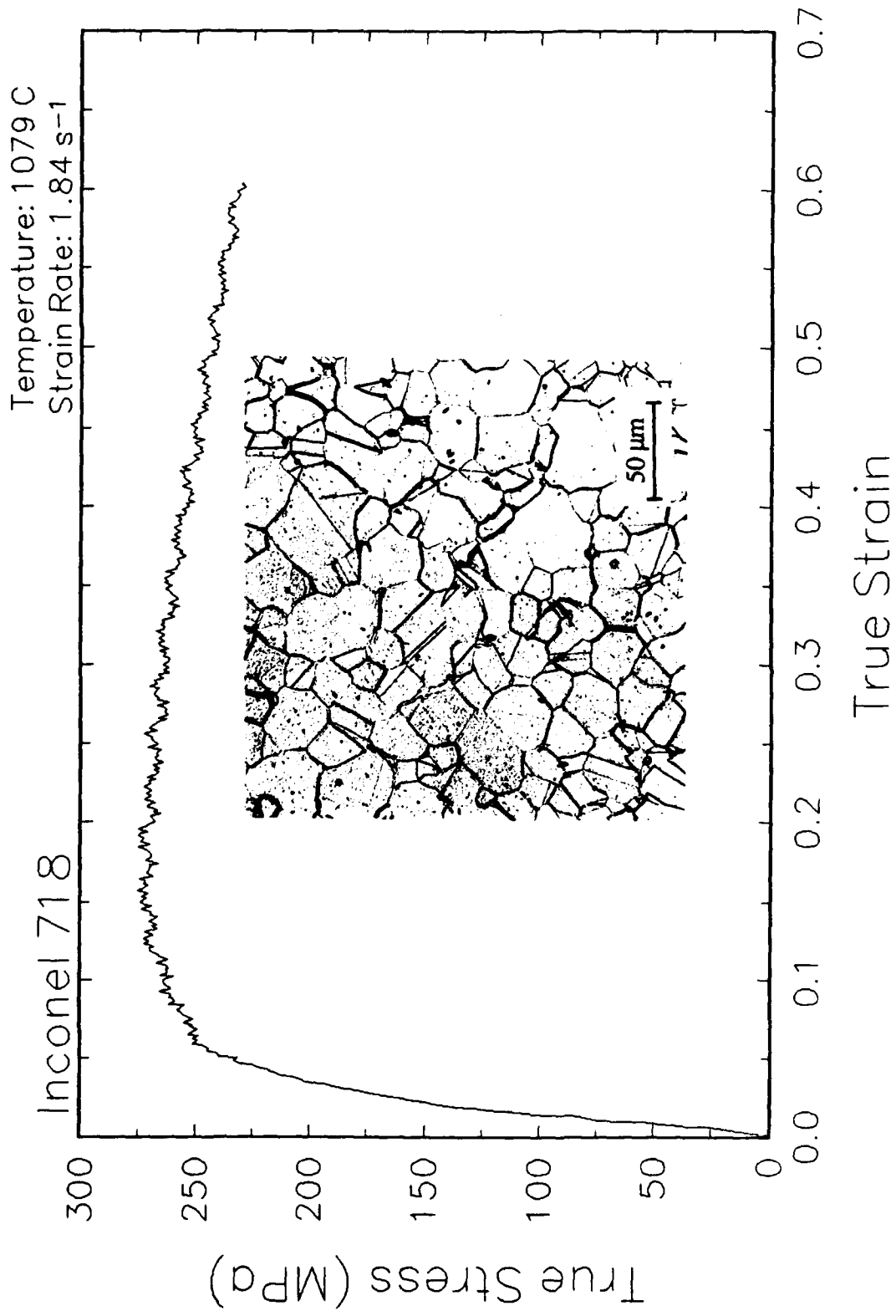Figure 12. True stress-true strain curve and microstructure at 1038 C and 0.01 s⁻¹.

Figure 13. True stress-true strain curve and microstructure at 1038 C and 0.14 s⁻¹.

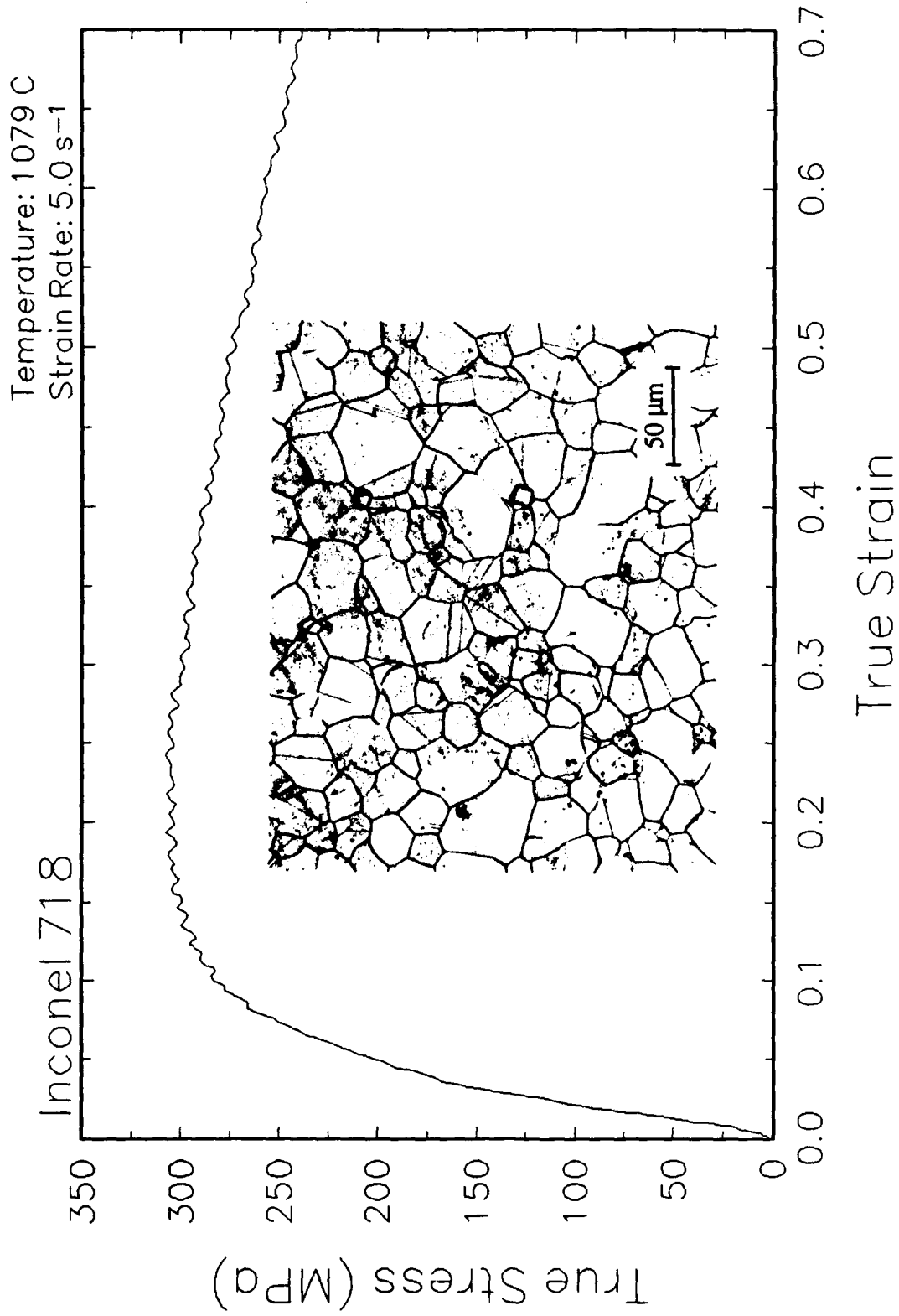Figure 14. True stress-true strain curve and microstructure at 1038 C and 1.84 s^{-1}.

Figure 15. True stress-true strain curve and microstructure at 1038 C and 5 s^{-1}.

Figure 16. True stress-true strain curve and microstructure at 1038 C and 25 s⁻¹.

Figure 17. True stress-true strain curve and microstructure at 1079 C and 0.01 s^{-1}.

Figure 18. True stress-true strain curve and microstructure at 1079 C and 0.14 s^{-1}.

Figure 19. True stress-true strain curve and microstructure at 1079 C and 1.84 s^{-1}.

Figure 20. True stress-true strain curve and microstructure at 1079 C and 5 s⁻¹.

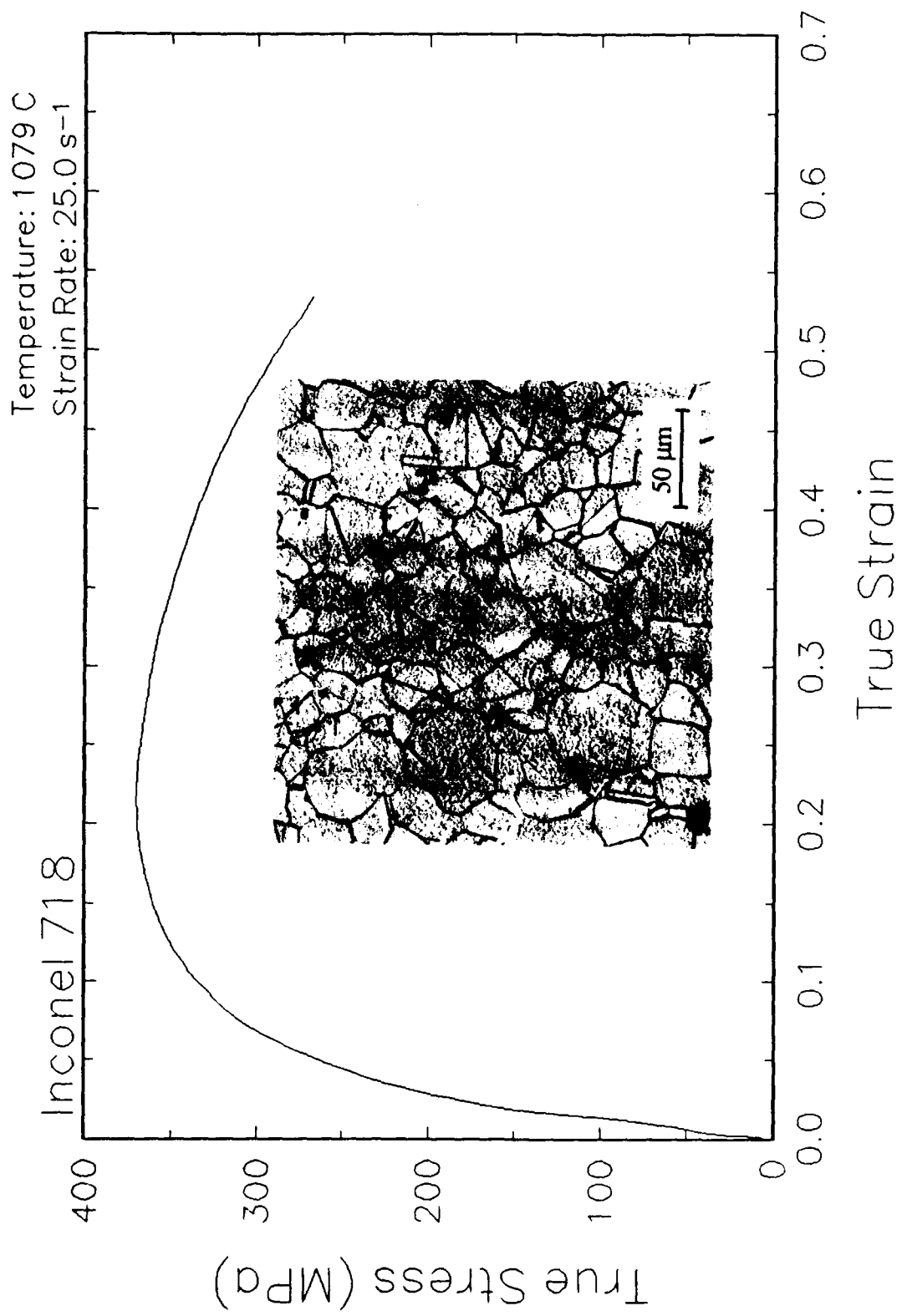Figure 21. True stress-true strain curve and microstructure at 1079 C and 25 s⁻¹.
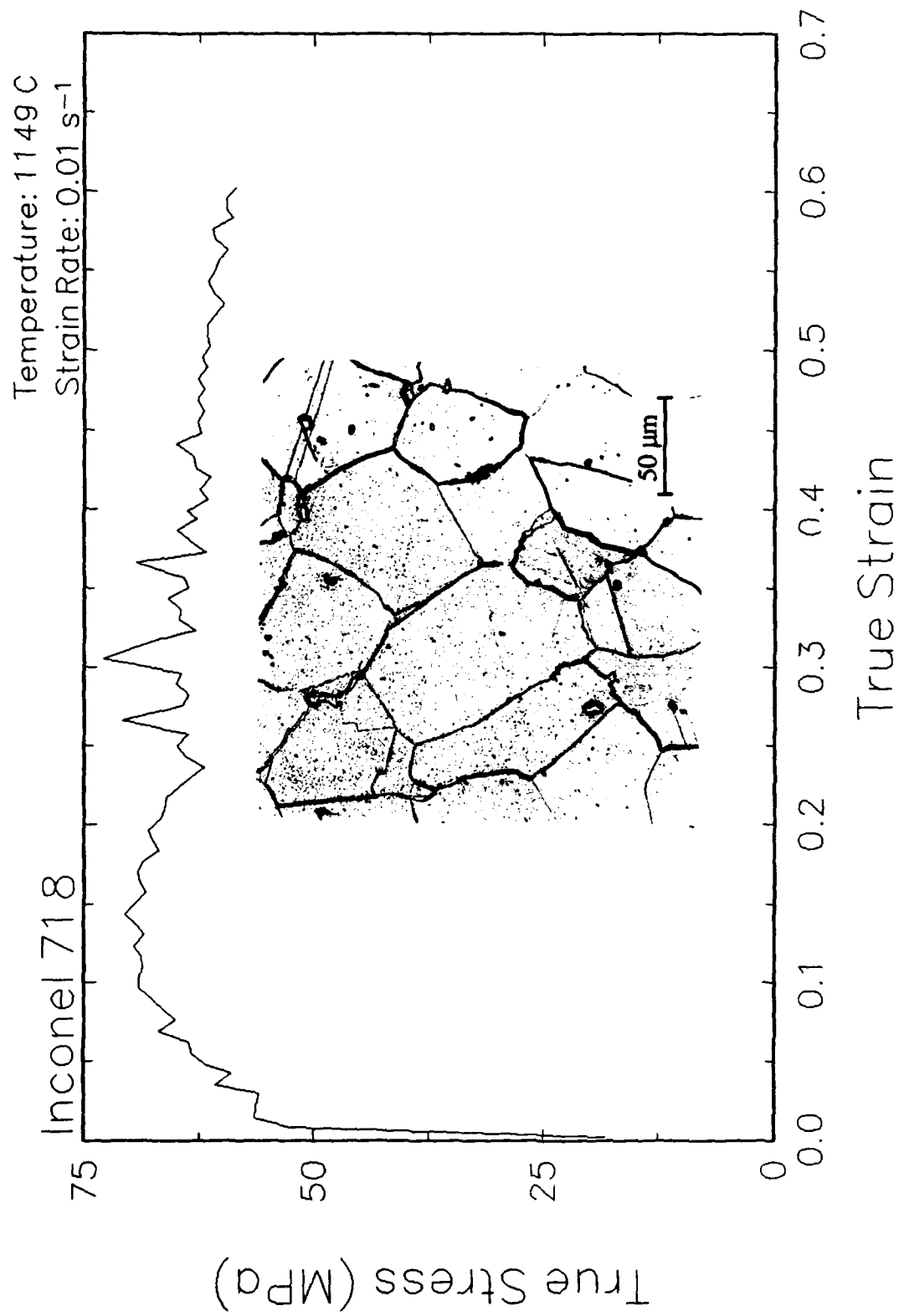
Figure 22. True stress-true strain curve and microstructure at 1149 C and 0.01 s⁻¹.
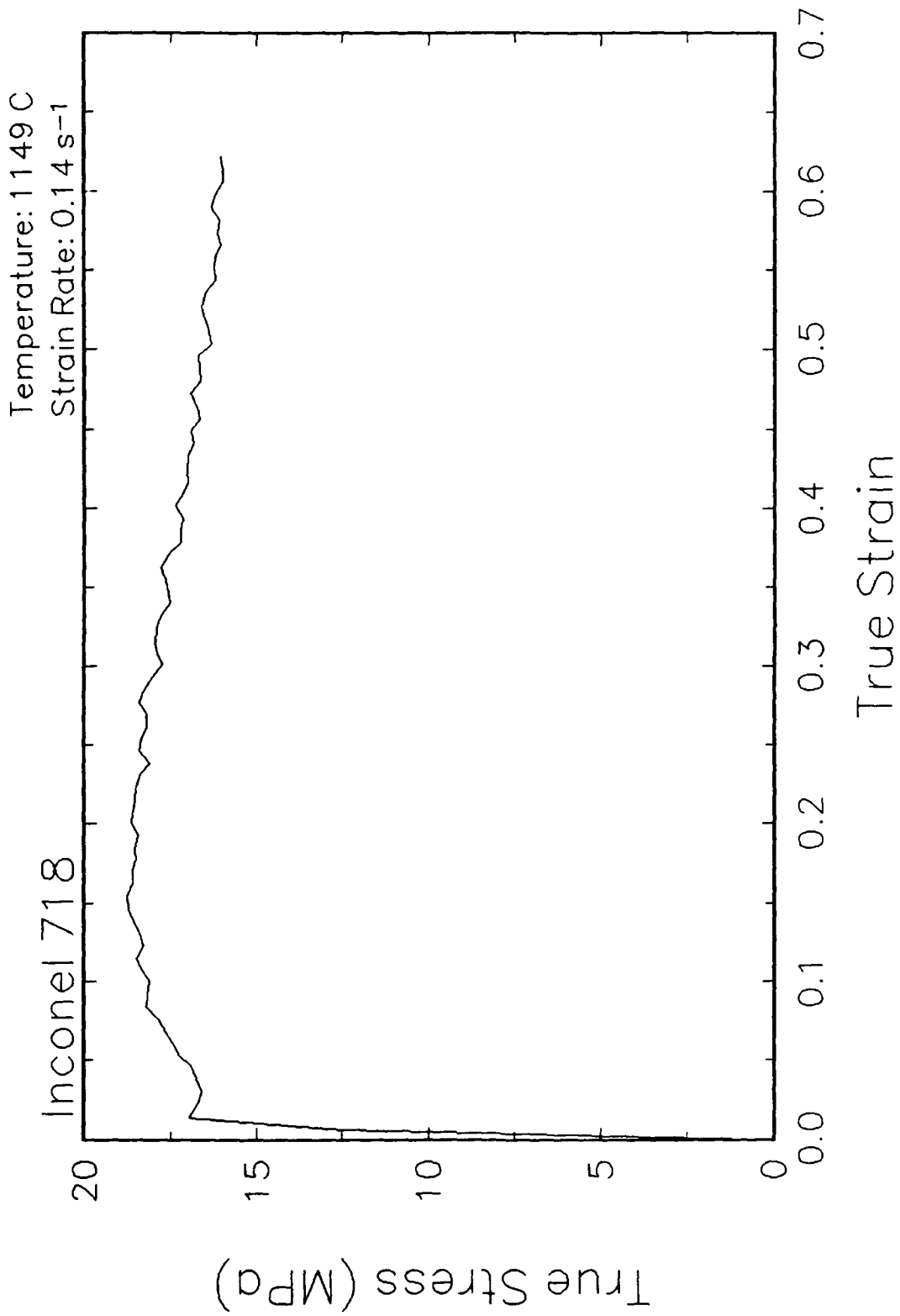
Figure 23. True stress-true strain curve and microstructure at 1149 C and 0.14 s⁻¹.
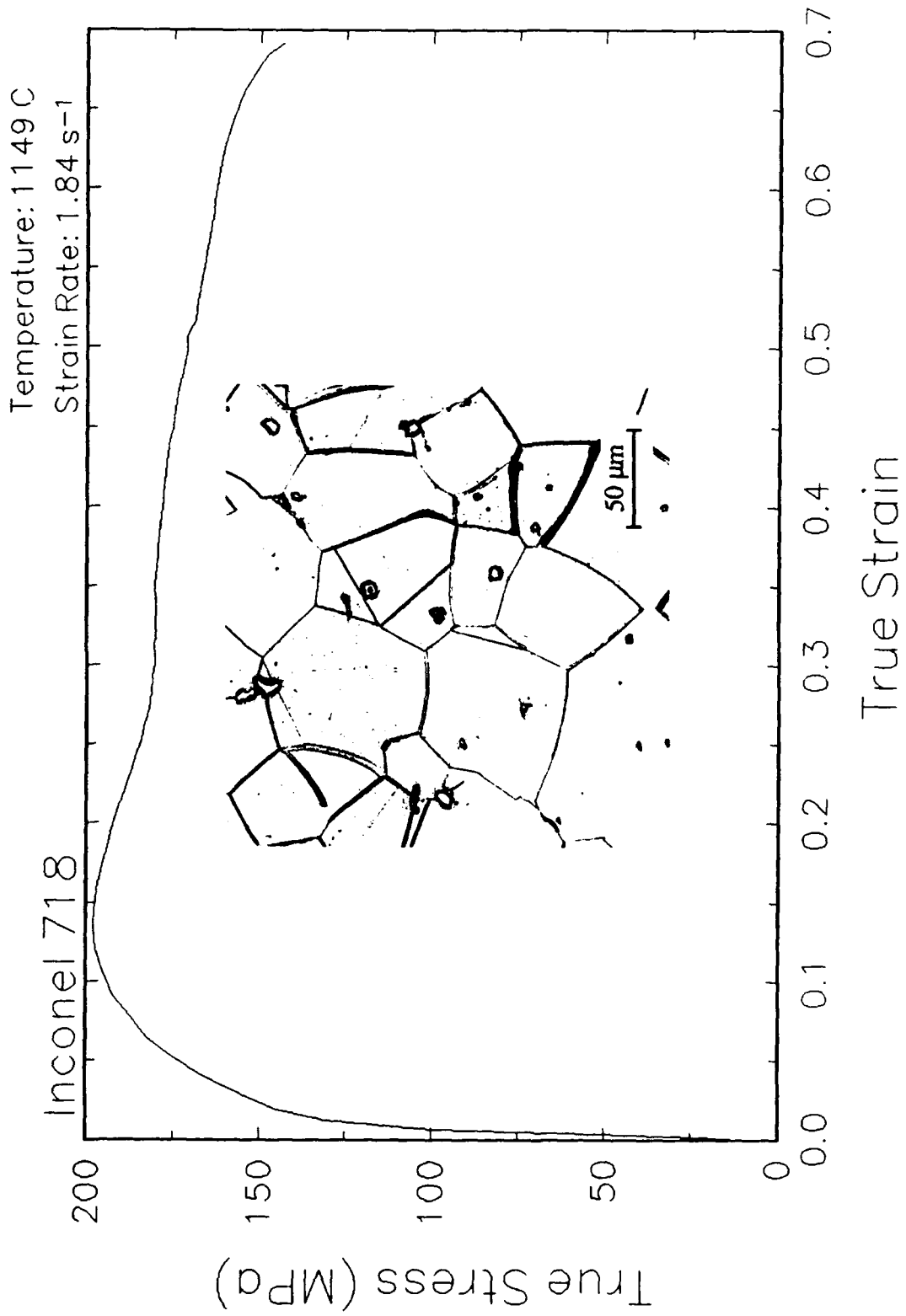
Figure 24. True stress-true strain curve and microstructure at 1149 C and 1.84 s⁻¹.
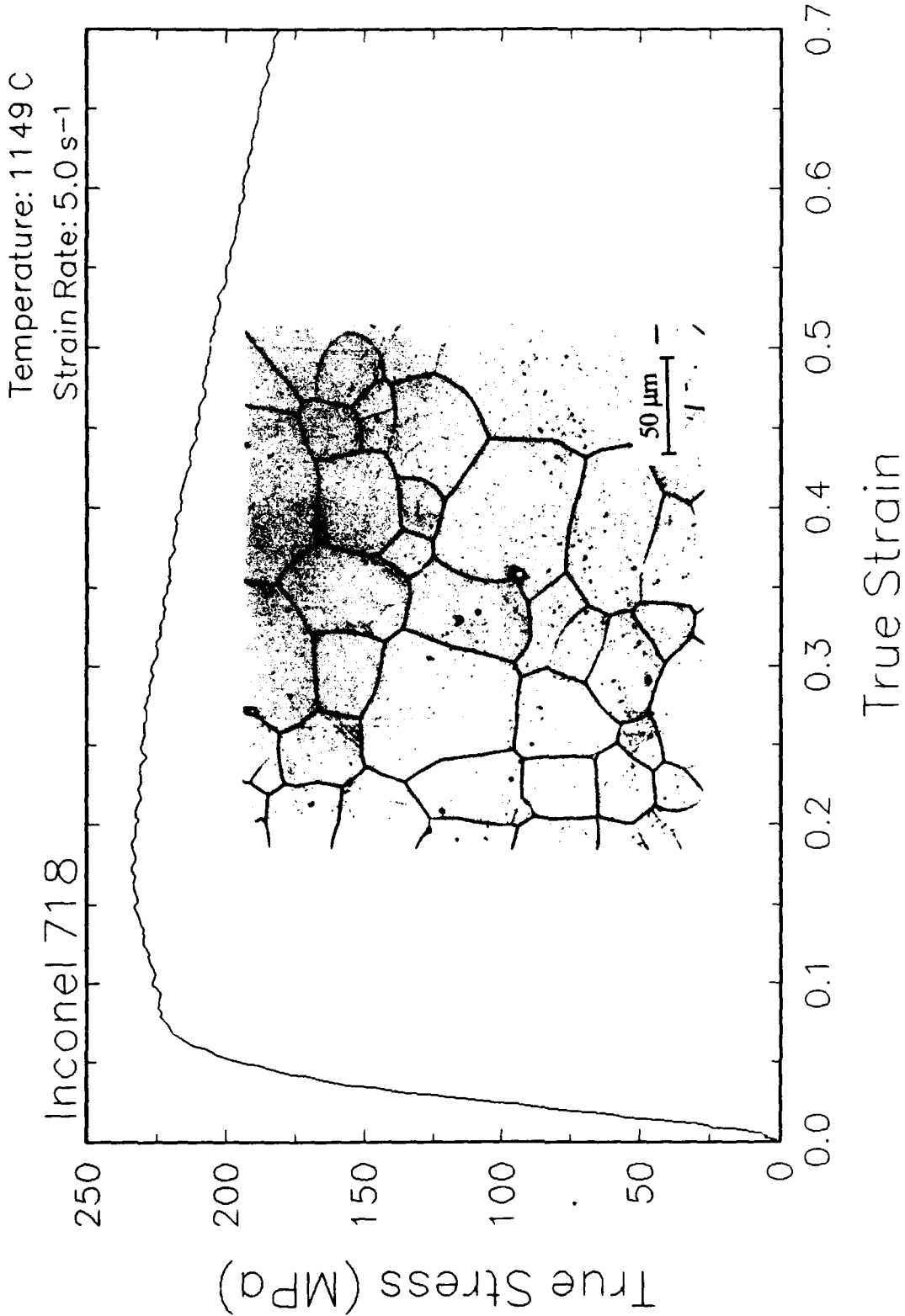
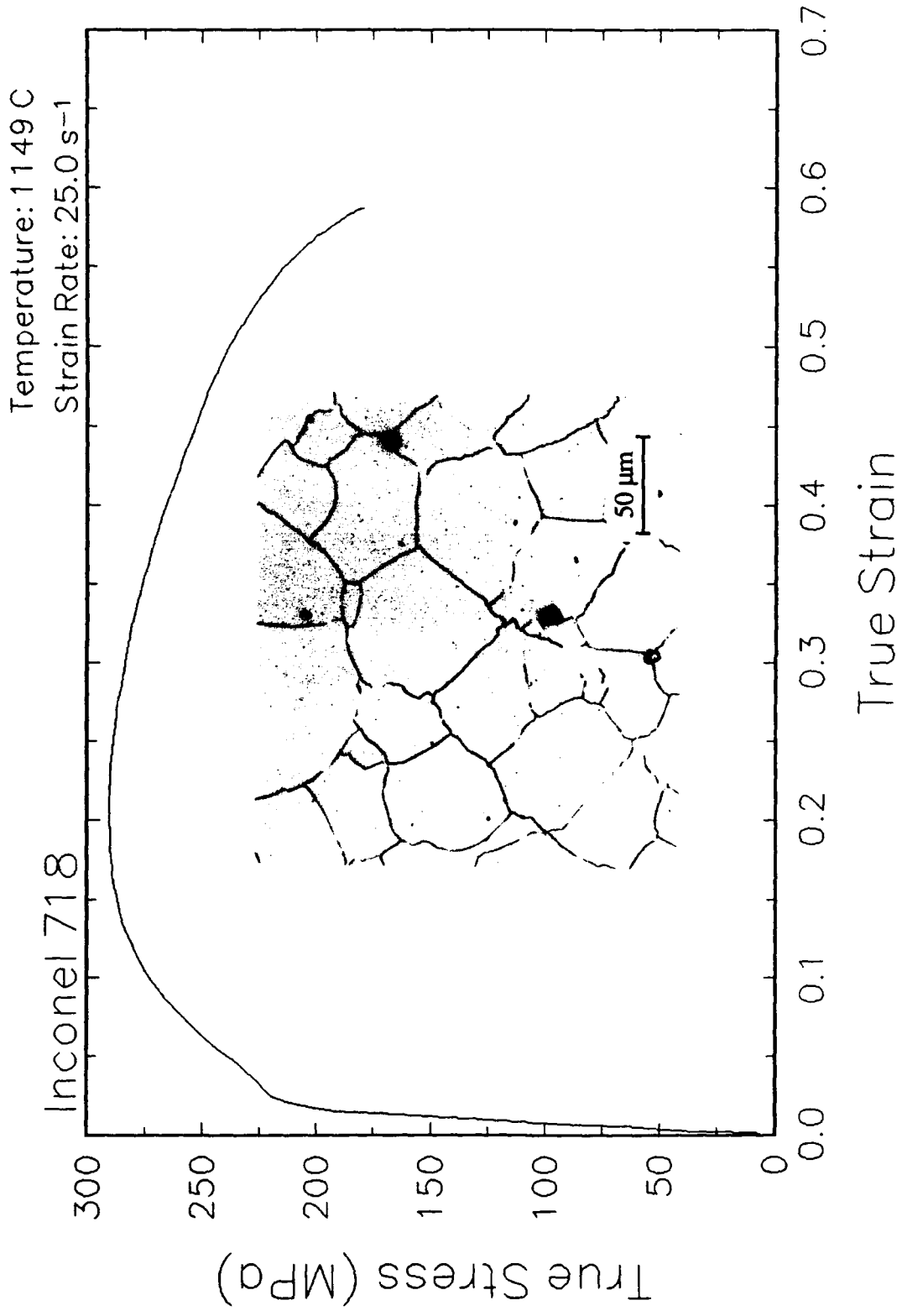Figure 25. True stress-true strain curve and microstructure at 1149 C and 5 s^{-1}.

Figure 26. True stress-true strain curve and microstructure at 1149 C and 25 s⁻¹.
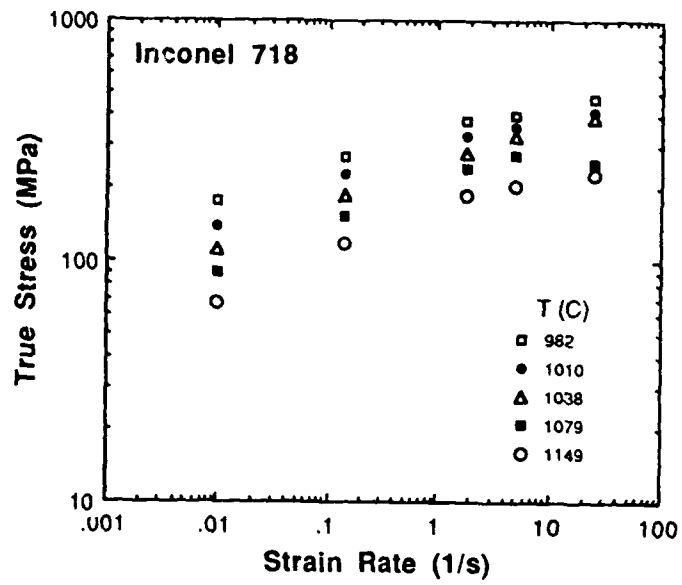
Figure 27. Effect of strain rate on stress in log-log scale at a true strain of 0.3 for Inconel 718.
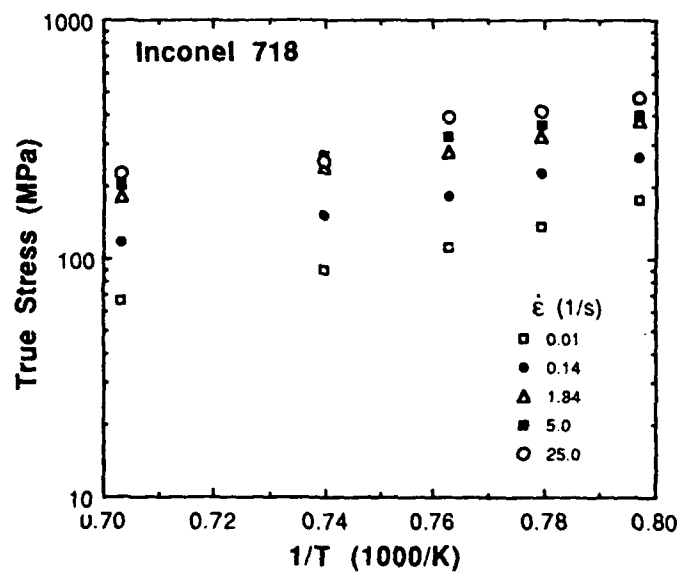

Figure 28. Effect of temperature on stress at a true strain of 0.3 for Inconel 718.
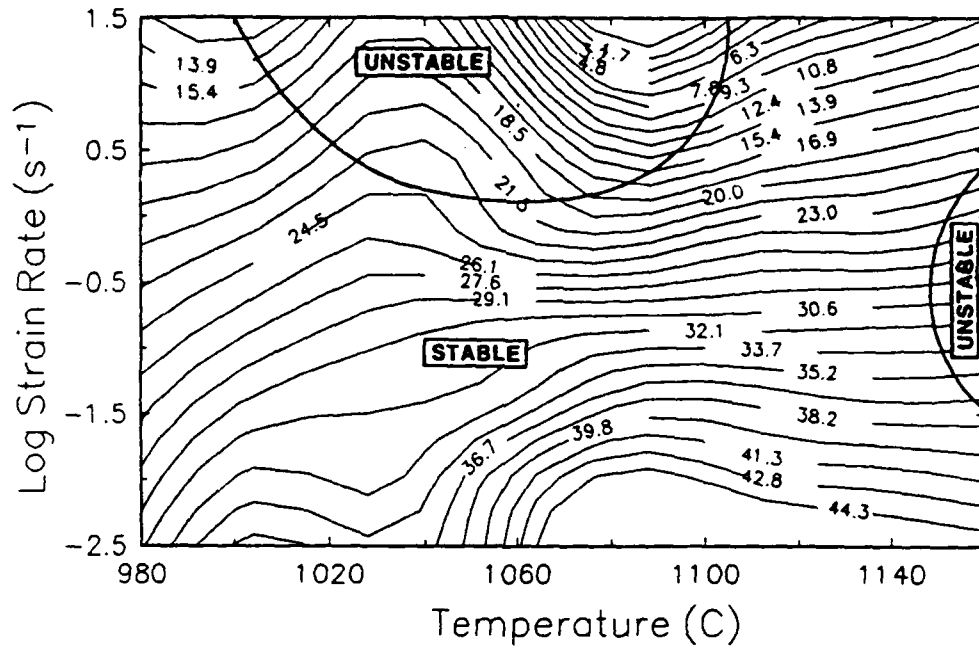
Figure 29. Processing map of Inconel 718 at a true strain of 0.3.

Summary

Compression tests have been performed on Inconel 718 over a range of temperatures and strain rates. The experimental conditions used in this work are representative of those used in metalforming practices. From the stress-strain curves, the flow behavior was characterized and a processing map indicating the optimum processing condition was generated. This condition is approximately 1070 C and 0.01 s^{-1}.

The deformed microstructures were characterized from the quenched specimens by optical microscopy and are presented for each testing condition under the stress-strain curves. Dynamic recrystallization and grain growth occurred over the temperature and strain rate range tested.

Implementation of Data Provided by the Atlas of Formability

The Atlas of Formability program provides ample data on flow behavior of various important engineering materials in the temperature and strain rate regime commonly used in metalworking processes. The data are valuable in design and problem solving in metalworking processes of advanced materials. Microstructural changes with temperature and strain rates are also provided in the Bulletin, which helps the design engineer to select processing parameters leading to the desired microstructure.

The data can also be used to construct processing map using dynamic material modeling approach to determine stable and unstable regions in terms of temperature and strain rate. The temperature and strain rate combination at the highest efficiency in the stable region provides the optimum processing condition. This has been demonstrated in this Bulletin. In some metalworking processes such as forging, strain rate varies within the workpiece. An analysis of the process with finite element method (FEM) can ensure that the strain rates at the processing temperature in the whole workpiece fall into the stable regions in the processing map. Furthermore, FEM analysis with the data from the Atlas of Formability can be coupled with fracture criteria to predict defect formation in metalworking processes.

Using the data provided by the Atlas of Formability, design of metalworking processes, dynamic material modeling, FEM analysis of metalworking processes, and defect prediction are common practice in Concurrent Technologies Corporation. Needs in solving problems related to metalworking processes can be directed to Dr. Prabir K. Chaudhury, Manager of the Atlas of Formability project, by calling (814) 269-2594.